



Differential bacterial capture and transport preferences facilitate co-growth on dietary xylan in the human gut

Leth, Maria Louise; Ejby, Morten; Workman, Christopher; Ewald, David Adrian; Pedersen, Signe Schultz; Sternberg, Claus; Bahl, Martin Iain; Licht, Tine Rask; Aachmann, Finn Lillelund; Westereng, Bjørge; Abou Hachem, Maher

Published in:
Nature Microbiology

Link to article, DOI:
[10.1038/s41564-018-0132-8](https://doi.org/10.1038/s41564-018-0132-8)

Publication date:
2018

Document Version
Peer reviewed version

[Link back to DTU Orbit](#)

Citation (APA):

Leth, M. L., Ejby, M., Workman, C., Ewald, D. A., Pedersen, S. S., Sternberg, C., ... Abou Hachem, M. (2018). Differential bacterial capture and transport preferences facilitate co-growth on dietary xylan in the human gut. Nature Microbiology. DOI: 10.1038/s41564-018-0132-8

General rights

Copyright and moral rights for the publications made accessible in the public portal are retained by the authors and/or other copyright owners and it is a condition of accessing publications that users recognise and abide by the legal requirements associated with these rights.

- Users may download and print one copy of any publication from the public portal for the purpose of private study or research.
- You may not further distribute the material or use it for any profit-making activity or commercial gain
- You may freely distribute the URL identifying the publication in the public portal

If you believe that this document breaches copyright please contact us providing details, and we will remove access to the work immediately and investigate your claim.

1 Differential bacterial capture and transport preferences facilitate 2 co-growth on dietary fibers in the human gut

3 Maria Louise Leth¹, Morten Ejby¹, Christopher Workman¹, David Adrian Ewald¹, Signe Schultz Pedersen¹, Claus Sternberg¹,
4 Martin Iain Bahl², Tine Rask Licht², Finn Lillelund Aachmann³, Bjørge Westereng⁴, Maher Abou Hachem^{1*}

5 1. Dept. of Biotechnology and Biomedicine, Technical University of Denmark, DK-2800 Kgs. Lyngby, Denmark. 2. National Food Institute,
6 Technical University of Denmark, DK-2800 Kgs. Lyngby, Denmark 3. NOBIPOL, Department of Biotechnology and Food Science, NTNU
7 Norwegian University of Science and Technology, N-7491 Trondheim, Norway, 4. Faculty of Chemistry, Biotechnology and Food Science,
8 Norwegian University of Life Sciences, N-1432 Ås. *e-mail: maha@bio.dtu.dk

9

10 Abstract

11 Metabolism of dietary glycans is pivotal in shaping the human gut microbiota. The mechanisms that
12 promote competition for glycans amongst gut commensals, however, remain unclear. *Roseburia*
13 *intestinalis*, an abundant butyrate-producing Firmicute, is a key degrader of the major dietary fiber
14 xylan. Despite the association of this taxon to a healthy microbiota, insight is lacking into its glycan
15 utilization machinery. Here, we investigate the apparatus that confers *R. intestinalis* growth on
16 different xylans. *R. intestinalis* displays a large cell-attached modular xylanase that promotes
17 multivalent and dynamic association to xylan via three known and one novel xylan-binding module.
18 This xylanase operates in concert with an ATP-binding cassette (ABC) transporter to mediate break-
19 down and selective internalization of xylan-fragments. This apparatus supports co-growth between
20 *R. intestinalis* with a model xylan-degrading *Bacterioides* in mixed cultures. The transport protein of
21 *R. intestinalis* prefers xylo-oligosaccharides of 4–5 xylosyl-units, whereas the counterpart from
22 competing *Bacterioides* targets larger ligands. This insight highlights the differentiation of capture
23 and transport preferences as a strategy to facilitate co-growth on abundant dietary fibers by gut
24 commensals. These findings offer a unique route to manipulate the microbiota based on glycan-
25 transport preferences in therapeutic interventions to boost or restore distinct taxa.

26 Introduction

27 The human gut microbiota (HGM) is recognized as a determinant of human health and metabolic
28 homeostasis^{1,2}. Specific signatures of the HGM are associated with local and systemic disorders
29 including irritable-bowel disease, obesity, type 2 diabetes and colon cancer³. The composition of the
30 HGM is greatly affected by dietary glycans, which are non-digestible by the host^{4,5}. Only a few
31 species out of the hundreds present in the HGM are equipped to deconstruct distinct complex
32 polysaccharides and ferment them into short chain fatty acids (SCFAs)⁶. The impact of SCFAs on host
33 health and physiology remains an important aspect of the microbiota-host interaction. Particularly
34 the SCFA butyrate, the preferred energy source for colonocytes, is known to have anti-inflammatory
35 roles and reduce the risk of colon cancer and enteric colitis⁷⁻¹⁰. Butyrate producers belonging to the
36 Firmicutes phylum are generally abundant in healthy individuals, but are markedly reduced in
37 patients with inflammatory disorders^{11,12}. Butyrate producers including *Roseburia* spp. are increased
38 in metabolic syndrome patients after faecal transfer therapy, and correlate positively to
39 improvement of insulin resistance¹³. Investigations of the metabolic preferences of butyrate
40 producers and their interplay with major HGM commensals are instrumental to develop therapeutic
41 interventions targeting butyrate-deficiency related disorders.

42 *Roseburia* is a common genus of *Clostridium* cluster XIVa within the Firmicutes that harbours
43 prevalent butyrate producers^{14,15}. This taxon adheres to mucin, consistent with an intimate
44 association with the host¹⁶. *Roseburia intestinalis* strains encode an impressive repertoire of
45 carbohydrate active enzymes (CAZymes) compared to most other Firmicutes¹⁷. *R. intestinalis*, the
46 taxonomically related *Eubacterium rectale* and species from the *Bacteroides* genus are the only
47 known HGM taxa that utilize the major hemicellulosic polysaccharide xylan¹⁸⁻²⁰. Xylan is particularly
48 abundant in cereal grains (arabinoxylan, AX), but is also found in fruits and vegetables
49 (glucuronoxylan, GX)²¹ (Fig. 1a). Xylan utilization by dominant gut commensals belonging to the

50 *Bacteriodes* genus has been investigated in detail^{22,23}, but similar knowledge is lacking for Firmicutes
51 counterparts.

52 Here, we show that *Roseburia intestinalis* L1-82 grows on acetyl, arabinosyl and 4-*O*-methyl-
53 glucuronosyl decorated dietary-relevant xylans, with a preference for cereal arabinoxylans. The
54 growth is mediated by a multi-modular cell-attached xylanase and by an ABC transporter. The gene
55 encoding this transporter was the most upregulated in response to xylan, consistent with a
56 paramount role during growth on this glycan. We have characterized the xylanolytic enzymes and
57 the transport protein, which enabled modelling xylan utilization by *R. intestinalis* and the
58 identification of two novel xylan-specific CAZyme families. *R. intestinalis* efficiently competes with a
59 model xylan degrader belonging to the genus *Bacteroides*, when grown on soluble and insoluble
60 xylans. A striking finding was that the transport proteins that confer xylo-oligosaccharides capture in
61 *R. intestinalis* and *Bacteroides* targeted ligands of different sizes, thus markedly reducing the
62 competition for preferred ligands by either taxon. These results emphasize the competitiveness of
63 butyrate producing Firmicutes in targeting key dietary fibers like xylan. The substantial differences in
64 transport proteins highlight the differential capture and transport preference as a key feature to
65 facilitate co-growth on abundant dietary fibres such as xylan.

66

67 Results

68 **Inducible cell-attached xylanase activity mediates growth of *R. intestinalis* on substituted xylans**

69 Anaerobic growth of *R. intestinalis* L1-82 was measured as an increase in OD_{600 nm} for growth on
70 soluble xylans and as a decrease in pH for growth on insoluble xylans (Fig. 1b-d). *R. intestinalis* L1-82
71 grows rapidly on soluble xylans with a preference for wheat arabinoxylan (WAX, $\mu_{\max}=0.26 \text{ h}^{-1}$)
72 compared to birch glucuronoxytan (BGX, $\mu_{\max}=0.13 \text{ h}^{-1}$) (Fig. 1c). Interestingly, this bacterium also
73 utilizes highly acetylated xylans and insoluble cereal arabinoxylans from wheat (InWAX) and oat
74 spelt (OSX), but not cornbran glucuronoarabinoxylan (CBX). Xylo-oligosaccharides and xylan-derived

75 monosaccharides (except glucuronic acid) were also utilized (Fig. 1b). Extracellular *endo*-1,4- β -
76 xylanase (hereafter referred to as xylanase) activity was induced upon growth on BGX, WAX, and
77 xylobiose (X2), despite poor growth on the latter disaccharide (Fig. 1e). The xylanase activity was
78 cell-attached, but was released upon treatment of the cells with a high salt concentration (Fig. 1f),
79 suggesting noncovalent attachment.

80

81 **Genes encoding an ABC transporter and a multi-modular xylanase are amongst the top**
82 **upregulated in response to growth of *R. intestinalis* on xylan**

83 To elucidate the genetic basis for growth on xylans, we performed an RNA-seq transcriptional
84 analysis of *R. intestinalis* grown on WAX, BGX, xylose and glucose. Of the 4777 predicted genes, 1–
85 3.5% were highly upregulated (Log2 fold-change > 5) on xylans compared to glucose (Supplementary
86 Table 1), the majority being involved in carbohydrate and energy metabolism. Besides a separate
87 locus encoding a multi-modular xylanase of glycoside hydrolase family 10 (GH10 according to the
88 CAZy classification, <http://www.cazy.org>²⁴), the top genes in the xylan transcriptomes cluster on a
89 single locus (Fig. 2a,b). This locus contains eleven genes including four xylanolytic CAZymes of GH43,
90 GH115, GH8, GH3. Only one (ROSINTL182_08192, LacI type, Pfam 00356) of three transcriptional
91 regulator genes was highly upregulated. Strikingly, the most upregulated gene in the xylan
92 transcriptomes encodes a solute binding protein (SBP) of an ABC transporter. Furthermore, the
93 genes encoding the permease components of this ABC transporter were amongst the top six
94 upregulated by xylans. Signal peptides were only predicted for the xylanase and the transporter SBP,
95 consistent with extracellular breakdown of xylan followed by capture and uptake of xylo-
96 oligosaccharides by the ABC transporter. The expression and the localization of the transport SBP
97 and the xylanase at the cell surface were corroborated using immunofluorescence microscopy (Fig.
98 2c). Two additional loci, unique to *R. intestinalis* L1-82, lacking in other *R. intestinalis* strains, were
99 also upregulated albeit markedly less (Supplementary Fig. 1a-d). One of these loci encodes a second

100 cell attached GH10 xylanase, which is also expressed at the cell surface (Supplementary Fig. 1e). The
101 transcriptomic analysis also enabled us to assign the ABC-transporter mediating xylose import and to
102 outline the genes involved in intracellular metabolism of xylose, arabinose and glucuronic acid
103 (Supplementary Fig. 1f,g).

104

105 **A new family of binding modules confers extended and dynamic xylan binding to the multi-**
106 **modular xylanase in *R. intestinalis***

107 The highly upregulated *RiXyn10A*, which is conserved within the *R. intestinalis* species, is one of the
108 largest known xylanases from human gut bacteria (Supplementary Fig. 2b). *RiXyn10A* comprises an
109 N-terminal unassigned domain (residues 28–165), a xylan binding module of CBM22, a catalytic
110 module of GH10, a tandem repeat of CBM9 xylan binding modules, a bacterial Ig-like domain group 2
111 (BIG2, pfam02368)²⁵ and a Listeria-Bacteroides repeat domain (LBR, pfam09479)²⁶. The two latter
112 domains likely mediate cell attachment of the enzyme to the cell^{25–27} in accordance with their
113 positive charge, which is compatible with binding to the negatively charged cell surface (residues
114 1100-1356, pI>10).

115 To generate insight into the unique modularity of *RiXyn10A*, we characterized the enzyme and
116 truncated versions thereof (Fig. 3a-d). *RiXyn10A* incubated with BGX, WAX and InWAX generated
117 linear and decorated oligosaccharides (Fig. 3b,c and Fig. 4). *RiXyn10A* was inactive on highly and
118 heterogeneously substituted arabinoglucuronoxylan from corn bran, consistent with the lack of
119 growth on this substrate by *R. intestinalis*. The enzyme was inactive on xylobiose (X2) and showed
120 very low activity on xylotriose (X3) (Supplementary Fig. 3a). By contrast, xyloetraose (X4) and
121 xylopentaose (X5) were hydrolyzed stoichiometrically, revealing the requirement for at least four
122 substrate-binding sub-sites for efficient hydrolysis.

123 A BLASTP search of the N-terminal unassigned domain (CBMx) against UniProt gave no hits
124 indicating the lack of homologues with assigned function. CBMx confers affinity to xylan as implied

125 from a two times higher K_M when this domain was deleted (Fig. 3d). Affinity electrophoresis
126 established CBMx to be a novel xylan-binding module and revealed a 30-fold stronger binding for
127 WAX compared to BGX (Fig. 3e,f and Supplementary Fig. 3c). Surface plasmon resonance (SPR)
128 analysis revealed the highest affinity towards xylohexaose (X6) consistent with the presence of a
129 binding cleft large enough to accommodate at least six xylosyl units (Fig. 3e,g and Supplementary
130 Fig. 4a-e). This analysis also indicated specificity to xylan as there was no measurable affinity to
131 mannohexaose (Man6). The relatively low binding affinity to X6 ($K_D \approx 0.5$ mM) was corroborated using
132 isothermal titration calorimetry (ITC) (Fig. 3e and Supplementary Fig. 4g,f). Deleting CBMx decreased
133 the average K_D of *RiXyn10A* from 128 μ M to 65.4 μ M (*RiXyn10A* Δ CBMx) (Fig. 3e and Supplementary
134 Fig. 4h-k), asserting that at least one or more of other CBMs possess higher affinity compared to the
135 N-terminal new module. Homologues (sequence identity 55–27%) of the new CBM are present
136 mainly in other bacteria from *Clostridium* XIVa cluster (Supplementary Fig. 4l), which merits the
137 assignment of these modules into a new CBM family.

138

139 **Preference of the binding protein of the ABC transporter that mediates uptake of xylan oligosaccharides in *R.***
140 ***intestinalis***

141 We showed above that the action of xylanases produces complex xylo-oligosaccharides likely decorated with
142 arabinosyl and 4-*O*-methyl-glucuronosyl. The presence of these decorations is supported by the decrease in
143 some of these peaks and the increase in arabinose and un-substituted xylo-oligosaccharides after treatment with
144 debranching enzymes (see next section). No oligosaccharides were detectable (HPAEC-PAD analysis, data not
145 shown) in spent supernatants from *R. intestinalis* growth on xylan, suggesting efficient uptake of oligomeric
146 products. The transcriptional analysis (Fig. 2a) identified an ABC transporter likely to mediate the uptake of the
147 xylo-oligosaccharides hydrolysis products of *RiXyn10A* from WAX and BGX. The preference of SBPs associated
148 with oligosaccharide-specific ABC transporters has been shown to correlate well to the uptake preference of
149 bacteria^{28,29}. We measured the affinity of *RiXBP*, the SBP of the upregulated ABC transporter, on a range of xylo-
150 oligosaccharide ligands (Table 1 and Supplementary Fig. 5). The preferred un-substituted ligand was X5

151 followed by X4, and the affinity decreased steeply for smaller or larger oligosaccharides. Internal
152 arabinosyl decorations (AX4) appeared to be preferred based on the 2.4-times higher affinity
153 compared to the un-substituted X4. The tolerance and recognition of arabinosylated ligands is in
154 agreement with the good growth on WAX. These results suggest that *RiXBP* is selective in capturing
155 internally branched xylo-oligosaccharides with a xylose backbone of 4–5 xylose residues.

156

157 ***R. intestinalis* degrades internalized decorated xylo-oligosaccharides by the concerted action of**
158 **three hydrolases and a novel family of acetyl esterases**

159 Xylo-oligosaccharides are degraded in the cytoplasm after their uptake. To gain insight into
160 intracellular xylan-oligosaccharide breakdown, we produced and characterized the α -glucuronidase
161 *RiAgu115A* (GH115), the α -L-arabinofuranosidase *RiAbf43A* (GH43), two xylosidases *RiXyl8* (GH8) and
162 *RiXyl3A* (GH3) as well as *RiAXE* (ROSITNL182_08194, GenBank accession EEU99941.1) from the core
163 xylan utilization locus.

164 *RiAgu115A* released 4-*O*-methyl-glucuronic acid (MeGlcA) from glucuronoxylans (BGX and BeGX) and
165 from BGX pretreated with *RiXyn10A* (Fig. 4a and Supplementary Fig. 6a-c). The k_{cat}/K_M of *RiAgu115A*
166 was 16-fold higher on glucuronoxylan hydrolysate compared to intact glucuronoxylan
167 (Supplementary Fig. 6c), indicating that *RiAgu115A* preferentially accommodates glucuronoxylo-
168 oligosaccharides, consistent with the intracellular localization of this enzyme. This enzyme also
169 cleaves MeGlcA decorations at the xylosyl penultimate to the reducing end (generated using a GH30
170 glucuronoxylanase, Supplementary Fig. 6b), but its activity was blocked by the presence of
171 acetylations (Fig. 4d).

172 *RiAbf43A* is an α -L-arabinofuranosidase that exclusively releases arabinose from WAX (Fig. 4a).
173 Kinetic analysis towards WAX and arabino-xylotetraose (AX4) (Supplementary Fig. 6d) revealed
174 recognition of internal arabinosyl substitutions, with a 13-fold increase in k_{cat} for oligosaccharides
175 consistent with the intracellular localization.

176 Both *RiXyl8* and *RiXyl3A* generated xylose from xylo-oligosaccharides, but lacked activity towards
177 xylan (Supplementary Fig. 6g-k). *RiXyl3A* degraded xylo-oligosaccharides completely into
178 monosaccharides, while *RiXyl8* was inactive towards X2. Reduction of xylo-oligosaccharides with
179 NaBH₄ abolished the activity of *RiXyl8* assigning it as a reducing-end β-xylosidase³⁰ (Supplementary
180 Fig. 6i), in contrast to *RiXyl3A* that recognizes non-reducing xylosyl moieties and maintains activity
181 on reduced xylo-oligosaccharides. Thus, the concerted and overlapping activities of these enzymes
182 (Supplementary Fig. 6) results in rapid depolymerization of arabinosyl and MeGlcA decorated xylo-
183 oligosaccharides.

184 *RiAXE*, which was un-assigned, based on lack of hits in a BLASTP search of UniProt, was highly
185 upregulated on xylans (Fig. 2a). This enzyme possesses the conserved residues in the SGNH lipases-
186 esterases superfamily (Pfam cd00229), which also includes CAZy carbohydrate esterase families CE2,
187 CE3, CE12 and CE16. We established that *RiAXE* is an acetyl esterase, but low sequence identities to
188 these families (<12%) merit assigning *RiAXE* into a new carbohydrate esterase family. Indeed
189 homologues of this enzyme are encoded by several *Clostridium* cluster XIVa strains from the human
190 gut and by a range of Firmicutes (Supplementary Fig. 7i).

191 Assaying *RiAXE* activity towards AcBGX oligosaccharides (generated with *RiXyn10A*) using NMR
192 revealed efficient deacetylation of both C2 and C3, but with a preference for C2 decorations (Fig. 4b
193 and Supplementary 7). Analysis of the deacetylation by MALDI-ToF MS left a single acetyl group on
194 the AcBGX oligosaccharides (Fig. 4e). Inclusion of *RiAgu115A* in this reaction resulted in complete
195 deacetylation (Fig. 4f) suggesting that the presence of MeGlcA decorations protects acetylations in
196 the proximity of the MeGlcA unit. Analysis of the deacetylation rates also unveiled the concerted
197 action with *RiAgu115A* and the preference to hydrolysates of *RiXyn10A* rather than intact xylan
198 (Supplementary Fig. 7c,d). *RiAXE* specifically recognizes acetylations on xylosyl units based on lack of
199 activity on acetylated chitin and very low activity on acetylated mannan and cellulose monoacetate

200 (Supplementary Fig. 7h). Taken together, the results showed that *Ri*AXE is an efficient xylan specific
201 representative of a new acetyl esterase family.

202 In summary of the biochemical characterization presented above, we propose a model for the
203 uptake and degradation of diet-derived acetylated arabinoxylan and glucuronoxylan by *R. intestinalis*
204 L1-82 (Fig. 5a).

205

206 ***R. intestinalis* competes with *Bacterioides* for xylans**

207 The growth potential of *R. intestinalis* was compared with the efficient xylan degrader *Bacterioides*
208 *ovatus*²², by observing growth of individual cultures and in co-culture. Both strains displayed similar
209 growth on xylan as carbon source (Fig. 5b-d and Supplementary Fig. 8a,b). In competition, both
210 strains appeared to grow equally well on xylans (Fig. 5e-g), whereas *R. intestinalis* dominated the co-
211 culture on X4 after 7 hours of growth (Fig. 5h). The results indicate that *R. intestinalis* is an efficient
212 primary degrader of xylan that is able to compete with *B. ovatus* and even outcompete this
213 bacterium on preferred smaller xylo-oligosaccharides.

214

215 Discussion

216 The human gut is dominated by bacteria from two phyla: the Gram-positive Firmicutes and the
217 Gram-negative Bacteroidetes. Firmicutes are generally regarded as metabolic specialists, while
218 Bacteroidetes (mainly from the *Bacterioides* genus) are considered generalists based on narrow
219 versus broad glycan utilization capabilities, respectively⁶. The size and diversity of encoded CAZymes
220 frequently reflects these metabolic labels. Although this generalization applies to *R. intestinalis*,
221 based on the relatively limited glycan growth profiles⁵, this species possesses distinctively larger
222 CAZymes than most known clostridial Firmicutes of the HGM¹⁷. *R. intestinalis* has been proposed as a
223 key xylan degrader in the human gut along with specific species of *Bacterioides*^{18,19}. Growth and
224 enumeration of *R. intestinalis* on dietary xylans including wheat bran is reported both *in vitro* and *in*

225 *vivo*^{20,32}. Insight is lacking, however, on the preferences and the molecular machinery evolved by *R.*
226 *intestinalis* to target xylan as compared to species of *Bacteriodes*. In this study, we present a model
227 that explains the molecular basis for the utilization of xylan by *R. intestinalis* L1-82 as a
228 representative for prevalent butyrate producing clostridia (Fig. 5a). Our data establish that *R.*
229 *intestinalis* is truly a primary degrader that is equipped with a highly efficient machinery for
230 utilization of complex dietary xylans, including insoluble arabinoxylan from cereals. Identified key
231 components of the *R. intestinalis* xylan utilization strategy include a multi-modular extracellular
232 xylanase and an ABC transporter, which confer the capture, breakdown and internalization of
233 decorated xylan oligosaccharides. In the cytoplasm, internalized xylo-oligosaccharides are
234 depolymerized without loss to competing species. We demonstrate the ability of *R. intestinalis* to
235 grow on acetylated xylan, which reflects an adaptation to this abundant decoration in dietary xylans
236 (Fig. 1b). Acetylated xylo-oligosaccharides are metabolized after internalization due to an
237 intracellular previously unknown esterase family capable of removing C2, C3 and double acetylations
238 (Fig. 4b and Supplementary Fig. 7).

239 The extracellular multi-modular xylanase *RiXyn10A*, the ABC transporter and enzymes conferring
240 cytoplasmic breakdown of xylan oligosaccharides were assigned as the core xylan utilization
241 apparatus of *R. intestinalis* (Fig. 2a,b). This assignment was based on i) conservation of this
242 apparatus within the *Roseburia* species (Supplementary Fig. 2a), ii) highest transcriptional
243 upregulation of the encoding genes on xylan (Fig. 2a), and iii) biochemical data from the present
244 study. The two additional xylan-upregulated loci in *R. intestinalis* L1-82 (Supplementary Fig. 1) are
245 lacking in *R. intestinalis* XB6B4 and *R. intestinalis* M50/1, both being able to grow on xylan²⁰. The
246 activity and expression of the xylanase *RiXyn10B*, encoded by one of these auxiliary loci
247 (Supplementary Fig. 3d), supports the participation of more than one locus in xylan breakdown in *R.*
248 *intestinalis* L1-82. Multiplicity of xylan utilization loci has been suggested to support targeting a
249 larger structural diversity of naturally occurring xylans by *Bacteriodes*²², which may also apply for *R.*
250 *intestinalis*.

251 Our data support the role of the *R. intestinalis* core xylanase *RiXyn10A* in mediating the capture and
252 breakdown of arabino- and glucuronoxylan (Fig. 1 and Fig. 3). This enzyme possesses four CBMs
253 from two known and one novel xylan-binding families, representing the most complex modular
254 organisation of HGM xylanases (Fig. 3a and Supplementary Fig. 2b). This organization is conserved
255 within the currently sequenced *R. intestinalis* species, while other *Clostridium* XIVa taxa possess
256 simpler enzymes lacking one or more of the *RiXyn10A* CBMs. The N-terminal CBMx of *RiXyn10A*
257 displays approximately 7-fold lower affinity for X6 than the average affinity measured for the
258 enzyme variant lacking this module (Fig. 3e). These data merit assigning this module into a novel
259 low-affinity xylan-specific CBM family. Nonetheless, CBMx is highly selective to arabinoxylan and
260 clearly contributes to the overall affinity of the enzyme (Fig. 3e). Low-affinity CBMs may potentiate
261 multivalent cooperative substrate binding, with minimal reduction of turn-over due to the energetic
262 penalty of bond-breaking during substrate displacement from the active site (*i.e* maintenance of a
263 relatively high k_{cat}/k_{off} ratio³³). The extended binding mediated by the CBMs of *RiXyn10A* seems to
264 confer an advantage in the capture and prolonged contact of the enzyme with xylan. Deletion of the
265 binding modules (*RiXyn10A-cata*) caused a substantial decrease in the apparent affinity towards
266 WAX and BGX as judged by the loss of curvature and deviation from Michaelis-Menten kinetics (Fig.
267 3d and Supplementary Fig. 3b). These findings are consistent with the importance of CBMs in
268 catalysis under substrate limitations. By contrast, similar turnover rates, were obtained by the
269 catalytic module and the full-length *RiXyn10A* at high (9 mg mL⁻¹) substrate concentrations
270 (Supplementary Fig. 3b). Multiplicity and variability of CBMs seem to be a signature of extracellular
271 enzymes from butyrate producing Firmicutes^{34,35}. By contrast, *Bacteriodes* members possess simpler
272 outer-membrane anchored GH10 xylanases with an inserted tandem CBM4 repeat within the
273 catalytic module²³. Xylan capture by *Bacteriodes*, however, is additionally orchestrated by moderate
274 affinity ($K_D \approx 60 \mu\text{M}$) xylan binding proteins that protrude away from the cell surface to facilitate
275 binding²².

276 *R. intestinalis* was able to compete with *B. ovatus* for xylans during the log-phase (Fig. 5e-g). Notably,
277 *R. intestinalis* seemed to outcompete *B. ovatus* after propagation of the co-culture (in the late log
278 phase) in fresh medium for two additional passages, which underscores the competitiveness of the
279 xylan utilisation machinery of this Firmicute (Supplementary Fig. 8c). *R. intestinalis* has been
280 reported to be associated to insoluble xylans, including wheat bran, while species of *Bacteriodes*
281 were enriched in the solubilized xylan fractions^{18,36}. The extended binding mediated by *RiXyn10A*
282 may play an important role in the association to insoluble substrates. Indeed, the expression of this
283 enzyme appeared similarly high in the mono- and mixed xylan cultures with *B. ovatus*
284 (Supplementary Fig. 8e). These observations are different from the reported down-regulation of
285 hydrolases by *Eubacterium rectale*, which is close taxonomic relative to *Roseburia*, during co-growth
286 with *Bacteriodes thetaiotamicron* on a fiber rich diet in previously germ-free mice³⁷.

287 The gene encoding the binding protein (*RiXBP*) of the ABC transporter that confers xylo-
288 oligosaccharide uptake in *R. intestinalis* was the most upregulated in the xylan transcriptomes,
289 attesting the crucial role of oligosaccharide capture and transport in the densely populated gut
290 ecological niche. The narrow preference of this protein for decorated backbone of 4–5 xylosyl units
291 aligned with the products of *RiXyn10A* (Fig. 3b and Fig. 4c). The affinity and size preference of *RiXBP*
292 were found to be very different from the corresponding protein from *Bifidobacterium*²⁹, which
293 prefers shorter xylo-oligosaccharides with a different side chain decoration pattern. Importantly,
294 striking differences in binding affinities and preference are observed when *RiXBP* is compared to the
295 SusD-like xylan-binding counterpart from *Bacteriodes*. Indeed, both SusD-like proteins from *B.*
296 *ovatus*, which mediate capture and internalization of xylan-oligosaccharides \geq X6 by SusC TonB-
297 dependent permeases, displayed no measurable binding to X4 and X5²², the preferred ligands of
298 *RiXBP*. These differential transport protein preferences are likely to be instrumental in establishing
299 competitive uptake profiles to select oligosaccharides of specific sizes and decorations for each
300 taxon. This is supported by the dominance of *R. intestinalis* when the co-culture with *B. ovatus* was
301 grown on X4 (Fig. 5h).

302 Our study highlights the molecular apparatus that *R. intestinalis*, as a model *Clostridium* group XIVa
303 Firmicute, has evolved to compete for abundant dietary glycans with other dominant commensal
304 bacteria. Strikingly complex enzymes with multiple ancillary modules mediate multivalent substrate
305 capture and breakdown. Highly over-expressed ABC transporters mediate efficient capture and
306 uptake of xylan oligosaccharides with a different preference than the corresponding transport
307 systems of currently known competing taxa. Based on these findings we propose that the
308 differentiation of glycan capture and uptake preferences represents an adaptation strategy to
309 facilitate co-growth and minimize competition for break down oligomers from major dietary fibers
310 by different human gut taxa.

311 This study gives insight into the mechanism that enables co-growth of prevalent human gut
312 commensals on the same dietary fiber and sets the stage for the design of better therapeutic
313 strategies aiming at restoring or boosting specific taxonomic groups in a safe and more controlled
314 manner than currently possible.

315

316 **Methods**

317 **Chemicals**

318 All chemicals were of analytical grade. Birchwood glucuronoxylan (BGX), beechwood glucuronoxylan
319 BeGX), corncob xylo-oligosaccharides (CCXOS) and xylose were from Carl Roth (Karlsruhe, Germany).
320 Cornbran xylan (CBX) was a kind gift from Dr. Madhav, Yadav, United States Department of
321 Agriculture, Agricultural Research Service. Soluble wheat arabinoxylan (low viscosity 10 centiStokes
322 (cSt)) (WAX), insoluble wheat arabinoxylan (high viscosity 48 cSt) (InWAX), xylobiose through to
323 xylohexaose (X2–X6), arabinoxylotriose (AX3), arabinoxylotetraose (AX4) and mannohexaose
324 (Man6) were from Megazyme (Wicklow, Ireland). D-Glucuronic acid was from Sigma Aldrich (St.
325 Louis, MO, USA). L-arabinose was from VWR International Ltd (Lutterworth, Leicestershire, UK). Xylo-

326 oligosaccharides Longlive 95P (XOS) were from Shandon Longlive Bio-technology (Shandong, China).
327 Acetylated birchwood glucuronoxylan (AcBGX), acetylated aspen glucuronoxylan (AcAGX), acetylated
328 spruce galactoglucomannan (AcSGGM) were prepared with steam explosion as previously
329 described³⁸. Cellulose acetate was a kind gift from Alexander Deutschle, University of Hamburg,
330 Germany. Acetylated chitin-oligosaccharides were prepared as previously described³⁹.

331

332 **Growth experiments and RNA-seq transcriptional analysis**

333 *R. intestinalis* DSM 14610 was grown in a Whitley DG250 Anaerobic Workstation (Don Whitley, UK)
334 in YCFA medium¹⁴ supplemented with autoclaved-sterilized 0.5% (w/v) carbohydrates. Cultures
335 (5mL) were grown in triplicates and OD_{600 nm} and pH (for insoluble substrates) were measured to
336 assess bacterial growth until the stationary phase was reached. Growth rates were calculated from
337 the exponential growth phase.

338 For the RNA-seq analysis, total RNA was extracted at mid- to late-log phase (OD_{600 nm} = 0.5–0.7) from
339 biological triplicate cultures (10 mL) grown in YCFA supplemented with 0.5% (w/v) glucose, xylose,
340 WAX or BGX. Cells were harvested (4000 g, 5 min, room temperature) and the pellets were frozen at
341 -80°C until RNA extraction. The RNA was extracted using the RNeasy Mini Kit (Qiagen) according to
342 the manufacturer's protocol after enzymatic lysis followed by mechanical disruption of the cells. A
343 DNase treatment was included to ensure removal of DNA. The purity and quantity of the extracted
344 RNA were assessed by an Agilent 2100 Bioanalyzer (Agilent Technologies, UK). Removal of ribosomal
345 RNA and library construction for RNAseq were performed using the ScriptSeq™ Complete Kit
346 (Epicentre). High-throughput sequencing was performed in a single lane in paired end reads on an
347 Illumina Hiseq 4000 platform at BGI (Copenhagen, Denmark). In total, 400 million paired-end reads
348 were obtained and the read quality was assessed by FastQC v0.11.5
349 (<http://www.bioinformatics.babraham.ac.uk/projects/fastqc/>). The R1 reads were chosen for
350 downstream analysis. Adaptor trimming and de-multiplexing was performed using custom python

351 scripts (based on the Biopython SeqIO module⁴⁰) and the FASTX-Toolkit v0.0.13.2
352 (http://hannonlab.cshl.edu/fastx_toolkit/). Reads were further trimmed with fastx_trimmer and
353 subsequently, filtered with fastq_quality_filter with minimum quality score 30 (-q 30) where 95% of
354 base-pairs meet the minimum quality score (-p 95). The resulting reads were kept if longer than 20
355 bps (-m 20). The *R. intestinalis* L1-82 reference genome and genome annotations are based on
356 assembly *GCA_000156535.1_ASM15653v1*, obtained from NCBI
357 (ftp://ftp.ncbi.nlm.nih.gov/genomes/genbank/bacteria/Roseburia_intestinalis/). Reads were
358 mapped to the reference genome using Tophat2^{41,42}, and gene counts were determined with
359 HTseq⁴³. Differential gene expression was performed using DeSeq2 in R⁴⁴.

360

361 **Xylanase activity measurements on whole cells**

362 Cell-associated xylanase activity was determined by growing *R. intestinalis* cells in 800 μ L YCFA
363 containing 0.5% (w/v) xylo-oligosaccharides, WAX, BGX or glucose for 15 hours. Cells were harvested
364 (4000 g, 5 min, room temperature), resuspended in phosphate-buffered saline (PBS) to $OD_{600\text{ nm}} = 0.3$
365 and xylanase activity was assayed using the DNS assay as described below. To determine the effect
366 of high ionic strength on the localization of xylanase activity, *R. intestinalis* cells were grown in 6 mL
367 YCFA containing 0.5% (w/v) BGX for 15 hours. Subsequently, the culture was divided into two 3 mL
368 aliquots and harvested as described above. Cell pellets were resuspended in 300 μ L PBS with or
369 without 1.5 M NaCl. The suspensions were spun down and both pellets and supernatants (wash
370 fractions) were collected. Cell pellets were washed with excess PBS and resuspended in 300 μ L PBS.
371 The xylanase activity of cells and wash fractions was assayed using the DNS assay.

372

373 **Expression and purification of *R. intestinalis* proteins mediating xylan utilization**

374 Open reading frames of the proteins without signal peptide, as predicted by SignalP v.3.0
375 (<http://www.cbs.dtu.dk/services/SignalP-3.0>), were amplified from *R. intestinalis* DSM 14610
376 genomic DNA using specific primers (Supplementary Fig. 9). Amplicons were cloned into the EcoRI
377 and NcoI restriction sites of a pETM-11 (kind gift from Dr. Gunter Stier, EMBL, Center for
378 Biochemistry, Heidelberg, Germany⁴⁵ or the XhoI and NcoI restriction site of a pET28a(+) (Novagen,
379 Darmstadt, Germany) using In-Fusion cloning (Takara) to express proteins as fusions with either
380 cleavable N-terminal His₆ tags or a C-terminal ones, respectively. Standard protocols were used for
381 recombinant protein expression and purification using His-affinity and size exclusion
382 chromatography.

383 **Enzymatic activity assays**

384 Enzymatic assays were carried out in a 50 mM HEPES 0.005% (v/v) Triton X-100, pH 7.0 standard
385 assay buffer unless otherwise stated. Hydrolysis kinetics of full-length or truncated xylanases
386 (10–200 nM) were assayed towards 1–9 mg mL⁻¹ of BGX, WAX or InWAX (37°C, 900 µL, 12 min).
387 Initial hydrolysis rates were determined by removing 200 µL aliquots every third minutes and
388 quenching the reaction in 300 µL 3,5-dinitrosalicylic acid (DNS) reagent⁴⁶. Next samples were
389 incubated for 15 min at 90°C followed by A_{540 nm} measurement in 96 microtitre plates. Xylose was
390 used as a standard (0–2.5 mM). Xylanase activity was assayed for *R. intestinalis* cells washed with
391 PBS ± 1.5 M NaCl, and wash-fractions, as above with the following modification: 180 µL of 1% (w/v)
392 BGX was incubated with 20 µL cell suspension or wash-fraction for 4 hours.

393 Hydrolysis kinetics of α-glucuronidase were analyzed on 1–9 mg mL⁻¹ BeGX or a hydrolysate thereof
394 (prepared by incubation with 4 mM RiXyn10A xylanase for 15 hours at 37°C followed by heat
395 inactivation). The initial rates of (*O*-methyl)-D-glucuronic acid release were measured using a
396 coupled enzymatic assay (Megazyme). Reactions (770 µL) were incubated for 2 min at 37°C with
397 10–180 nM enzyme with intermittent removal of 175 µL aliquots every 15 s into 125 µL 1 M Tris pH
398 10 to quench the reaction. This was followed by mixing 270 µL of the stopped reaction with 45 µL of

399 the NAD⁺ and uronate dehydrogenase reagents. Conversion of NAD⁺ to NADH was measured at A₃₄₀
400 nm. Glucuronic acid was used as standard (0–500 μM).

401 Hydrolysis kinetics of *RiXyl8* and *RiXyl3A* were determined towards xylobiose (X2) through to
402 xylohexaose (X6) (0.5–12 mM) in McIlvaine buffer pH 6.8 (10 mM citric acid and 20 mM sodium
403 phosphate) as described in^{47,48}. Reactions (350 μL) were incubated for 12 min at 37°C with 36–78 nM
404 *RiXyl3A* or 2.4 nM *RiXyn8*. Aliquots of 50 μL were removed every 2 minutes and stopped in 250 μL *p*-
405 bromoaniline (2% w/v) in glacial acetic acid with thiourea (4% w/v). The stopped reactions were
406 incubated in darkness for 10 min at 70°C, followed by incubation at 37°C for 1 hour before
407 measuring A_{520 nm}. The concentration of released pentoses was determined using a xylose standard
408 (0–5 mM)⁴⁹.

409 α-L-Arabinofuranosidase activity for *RiAbf43A* was assayed in McIlvaine buffer pH 6.8 (10 mM citric
410 acid and 20 mM sodium phosphate) using a coupled enzymatic L-arabinose/D-galactose assay
411 (Megazyme) towards WAX (1–24 mg mL⁻¹). Reactions (75 μL) were incubated for 12 min at 37°C with
412 0.4–1.7 μM enzyme. Aliquots of 15 μL were removed every 2 min, and the enzyme was inactivated
413 (10 min, 90°C) and thereafter 10 μL of this solution were mixed with 10 μL of the provided NAD⁺, 20
414 μL of provided assay buffer and 2 μL galactose mutaoatase/β-galactose dehydrogenase mix. The
415 formation of NADH was measured as above. Arabinose was used as standard (0–5 mM).

416 The acetyl esterase specific activity of *RiAXE* was determined in 250 μL reactions containing *para*-
417 nitrophenyl-acetate (4 mM) and 0.14 μM enzyme. A_{405 nm} was measured every 60 s for 10 minutes
418 at 37°C in a microtiter plate reader and *p*NP (0–1 mM) was used as standard. The specific activity
419 was determined in units (U/mg), where a U is defined as the amount of enzyme that produces 1
420 μmol of *p*NP min⁻¹.

421 Kinetic parameters were calculated by fitting the Michaelis-Menten equation to the initial rate data
422 using Graph Pad Prism 7. The catalytic efficiency k_{cat}/K_m , determined from the slope of the

423 normalized initial rate ($V_0/[E]$) in the Michaelis-Menten plot, is reported when saturation was not
424 attained. All experiments were performed in triplicates.

425 **Action patterns of individual and mixtures of xylanolytic enzymes**

426 Hydrolysis of xylan and xylo-oligosaccharides was performed at 37°C for 15 hours in the standard
427 assay buffer used above. Oligosaccharide hydrolysates, used to assay the sequential action of the
428 debranching xylanolytic enzymes, were generated using *RiXyn10A*, which was separated by
429 ultrafiltration (3 kDa cutoff) before the addition of debranching enzymes. The hydrolysis profiles
430 were analyzed as detailed below. To verify the mode of reducing-end attack of *RiXyl8*, 30 mg XOS in
431 standard assay buffer were reduced by NaBH_4 (1M in 100 μM NaOH). A total of 200 μL of the NaBH_4
432 was added dropwise to 800 μL of the xylo-oligosaccharides solution, which was kept on ice. As
433 control 100 μM NaOH was added to an 800 μL xylo-oligosaccharides solution. The mixture was
434 incubated 1 hour at room temperature, then quenched by 400 μL 1 M acetic acid and diluted 10x in
435 assay buffer.

436 **Matrix-assisted laser desorption-ionization (MALDI)**

437 Oligosaccharides were analyzed with an Ultraflex MALDI ToF/ToF instrument (Bruker Daltonics,
438 Bremen, Germany). The samples were applied with 2,5-dihydroxybenzoic acid (DHB) as matrix to a
439 MTP 384 ground steel target plate (Bruker Daltonics). All spectra were obtained in positive reflection
440 mode and processed using Bruker flexAnalysis 3.3.

441 **Thin layer chromatography (TLC) and High performance anion-exchange chromatography with** 442 **pulsed amperometric detection (HPAEC-PAD)**

443 Aliquots of 1 μL of enzymatic reactions were spotted on a silica gel 60 F254 plate (Merck, Germany).
444 The chromatography was performed in a butanol:acetic acid:water (2:1:1 v/v) mobile phase. The
445 plates were dried at 50°C and carbohydrate hydrolysis products were visualized by spraying with a 5-
446 methylresorcinol:ethanol:sulfuric acid (2:80:10 % v/v) developer and tarred briefly at 350°C until

447 bands appeared. Release of xylo-oligosaccharides and monosaccharides was analyzed by HPAEC-
448 PAD on an ICS-3000 (Dionex, CA, USA) using a 3x250mm CarboPac PA1 column, a 3x50 mm guard
449 column and 10 μL injections. Xylo-oligosaccharide and standards were eluted with mobile phase of
450 constant 0.1 mM NaOH (flowrate 0.35 mL min⁻¹) and a two-step linear gradient of sodium acetate;
451 0–25 min of 0–75 mM and 25–30 min of 75–400 mM. Monosaccharides and standards (0.1 mg mL⁻¹)
452 of galactose, arabinose, glucose and xylose were eluted with 1 mM KOH for 35 min at 0.25 mL min⁻¹.

453

454 **NMR spectroscopy**

455 For the time-resolved NMR recordings: 4 mg AcBGX or AcSGGM were dissolved in 500 μL 50 mM
456 phosphate buffer pH 7.0 (99.9% D₂O). 2.5 μL of *Ri*AXE to a final concentration of 64 nM was added.
457 The recorded spectrum is a pseudo-2D type experiment recording a 1D proton NMR spectrum every
458 5 min with in total 220 time points. The 1D proton spectrum was recorded with 24 scans using a 30°
459 flip angle, and relaxation delay of 1 s (total recording time of 73 s). For enzyme treatment, 2.5 μL of
460 *Ri*Xyn10A and *Ri*Agu115A were added to the AcBGX sample to 167 nM and 13 nM, respectively, and
461 the sample incubated at 37°C for 24 hours prior to *Ri*AXE addition. All homo and heteronuclear NMR
462 experiments were recorded on a BRUKER AVIIIHD 800 MHz (Bruker BioSpin AG, Fälladen,
463 Switzerland) equipped with 5mm with cryogenic CP-TCI and all acquisitions were done at 37°C. For
464 chemical shift assignment of AcBGX, the following spectra were recorded: 1D proton, 2D double
465 quantum filtered correlation spectroscopy (DQF-COSY), 2D total correlation spectroscopy (TOCSY),
466 2D ¹³C heteronuclear single quantum coherence (HSQC), 2D ¹³C Heteronuclear 2 Bond Correlation
467 (H2BC), 2D ¹³C HSQC-[¹H,¹H]TOCSY and 2D heteronuclear multiple bond correlation (HMBC). The
468 acetate signal to 1.903 ppm (pH 7.0 at 37 °C, in relation to 4,4-dimethyl-4-silapentane-1-sulfonic
469 acid, DSS⁵⁰) was used as chemical shift reference for protons, while ¹³C chemical shifts were
470 referenced indirectly to acetate, based on the absolute frequency ratios⁵¹. The spectra were
471 recorded, processed and analyzed using TopSpin 3.5 software (Bruker BioSpin).

472

473 **Surface plasmon resonance (SPR)**

474 Xylo-oligosaccharide binding to *RiXyn10A*, *RiXyn10AΔCBMx* and *RiXyn10A-CBMx* was analyzed using
475 surface plasmon resonance (SPR) on a Biacore T100 (GE Healthcare). Immobilization of the proteins
476 on a CM5 chips was performed using a random amine coupling kit (GE Healthcare) according to the
477 manufacture's protocol with 50-150 $\mu\text{g mL}^{-1}$ protein in 10 mM sodium acetate pH 3.6-4.2, to a
478 density of 1362, 10531 and 4041 response units (RU) for *RiXyn10AΔCBMx*, *RiXyn10A* and *RiXyn10A-*
479 *CBMx*, respectively. The analysis comprised 90 s of association, 240 s of dissociation at 30 $\mu\text{L min}^{-1}$.
480 Sensograms were recorded at 25°C in 20 mM phosphate/citrate buffer, pH 6.5, 150 mM NaCl,
481 0.005% (v/v) P20 (GE Healthcare). All solutions were filtered prior to analysis (0.22 μm). Experiments
482 were performed in duplicates with seven concentrations in the range 156 μM –10 mM for X3, 75
483 μM –4 mM for X4, X6, Man6 and 62.5 μM –4 mM X5. Data analysis was carried out using the Biacore
484 T100 evaluation software and dissociation constants (K_D) were determined by fitting a one-binding
485 site model to the steady state sensograms. No binding was measured for Man6.

486 **Isothermal titration calorimetry (ITC)**

487 Titrations were performed using a Microcal ITC₂₀₀ calorimeter (GE healthcare) at 25°C with *RiXBP*
488 (0.1 mM) or *RiXyn10AΔCBMx* (0.25 mM) in the sample cell and xylo-oligosaccharides (2.2–5 mM) in
489 10 mM sodium phosphate pH 6.5 in the syringe. An initial injection of 0.5 μL , was followed by 19 x 2
490 μL injections separated by 120 s. The data were corrected for the heat of dilution, determined from
491 buffer titration and a nonlinear single binding model was fitted to the normalized integrated binding
492 isotherms using the MicroCal Origin software v7.0 to determine the thermodynamic binding
493 parameters.

494 **Affinity electrophoresis**

495 Binding of CBMx to WAX (0–0.1% w/v) or BGX (0–1.0% w/v) was assessed by affinity
496 electrophoresis⁵² in 10% native polyacrylamide gels (70 V, 3 hours, 4°C) using purified recombinant

497 *RiXyn10A*-CBMx (3.0 µg) and β-lactoglobulin (1.5 µg) as a negative control. The relative mobility (r)
498 was calculated as the migration of *RiXyn10A*-CBMx relative to migration of the dye front. A linear
499 regression of the 1/r versus xylan concentration allowed the determination of K_D as the intercept of
500 this X-axis.

501

502 **Western blot and immunofluorescence microscopy**

503 Custom antibodies against the recombinant for the two xylanases *RiXyn10A*, *RiXyn10B* and the
504 transport protein *RiXBP* were raised in rats and rabbit, respectively (Eurogentec, Seraing, Belgium).
505 The specificity of the antibodies was tested by western blots using a standard protocol. The
506 membranes were blocked for 1 hour in 1% (w/v) BSA in TBST-buffer (Tris-buffered saline, 0.1% (v/v
507 Tween 20) and incubated for 2 hours with the antisera (500x dilution in TBST-buffer). Subsequently,
508 the membranes were washed three times in TBST-buffer and incubated for 2 hours with 6000x
509 diluted secondary polyclonal goat anti-rabbit IgG-AP antibodies coupled to alkaline phosphatase (AP)
510 (Dako, Glostrup, Denmark) and rabbit anti-rat IgG-AP (Sigma). After three washes, the proteins were
511 visualized by exposure to Sigma-Fast BCIP/NBT reagent (Sigma).

512 *R. intestinalis* cells were grown in 6 mL YCFA containing 0.5% (w/v) WAX to $OD_{600\text{ nm}} \approx 0.8$, harvested
513 (4000 g, 5 min, room temperature) and washed twice in PBS. The cells were resuspended in 3 mL 4%
514 (w/v) paraformaldehyde in PBS and fixed by incubation on ice for 15 min. Thereafter the cells were
515 washed twice in PBS and resuspended in 2 mL PBS. 50 µL of cell suspension were added to glass
516 slides coated with poly-L-lysine, cells blocked for 1 hour in blocking buffer (1% (w/v) milk powder in
517 PBS) and washed twice in PBS. For labelling, the cells were incubated with 50 µL anti-sera diluted 50x
518 in blocking buffer for 2 hours, washed twice in PBS and incubated for 1 hour with 50 µL goat anti-rat
519 IgG Alexa-Fluor 555 or goat anti-rabbit IgG Alexa-Fluor 488 (Thermo Scientific, Massachusetts, USA).
520 Secondary antibodies were diluted 500x PBS. Finally, cells were washed two times in PBS, one drop
521 of ProLong Gold antifade (Thermo Scientific, Massachusetts, USA) was applied and the cells secured

522 with a cover slide. Fluorescence was visualized using Zeiss Axioplan 2 microscope equipped with a
523 CoolSNAP cf color camera and a Zeiss Plan-Neofluar 100X/1.3NA, oil immersion objective.

524

525 **Co-culture competition assay**

526 *Bacteriodes ovatus* DSM 1896 and *R. intestinalis* DSM 14610 were grown anaerobically in 20 mL
527 YCFA supplemented with 0.5% (w/v) glucose to late-log phase and an approximately equal number
528 of cells (estimated by OD_{600 nm}) were inoculated into CFA medium (YCFA lacking the yeast extract to
529 minimize *B. ovatus* growth on yeast extract⁵³) containing 0.5% (w/v) WAX, BGX, InWAX or X4. The
530 co-cultures were grown in triplicates and samples (2 mL) were taken during growth. In the
531 propagation experiment, the co-culture was passaged into fresh media after 9 hours of growth (start
532 OD_{600 nm}= 0.01), then grown for 12 hours and passaged again into fresh media and grown for 12
533 hours. Genomic DNA was extracted from samples using DNAClean® Microbial DNA isolation kit
534 (Qiagen). Relative bacterial abundance was estimated by qPCR. The extracted DNA was diluted to
535 0.5 ng µL⁻¹ and amplified in technical triplicates using strain specific primers (Supplementary Fig. 9)
536 The amplification mix contained 2 µl DNA, 5.5 µl LightCycler 480 SYBR Green I Master mix (Roche),
537 0.22 µL of each primer (10 pmol/µL) and 3 µL sterile water. Amplification conditions were 1 cycle of
538 95 °C for 5 min, 45 cycles of 95 °C for 10 s, 60 °C for 15 s and 72°C for 45 s using a LightCycler 480 II
539 (Roche). Relative bacterial concentrations in each sample were estimated by comparing the gene
540 copy numbers calculated using standard curves prepared with the respective reference DNA.
541 Western blot was performed as described above but with cell cultures instead of purified proteins.

542

543 **Data availability**

544 The protein characterized in this study are available from NCBI with the following accession
545 numbers: [EEV01588.1](#) (ROSINTL182_06494), [EEU99940.1](#) (ROSINTL182_08193), [EEU99941.1](#)
546 (ROSINTL182_08194), [EEU99942.1](#) (ROSINTL182_08195), [EEU99943.1](#) (ROSINTL182_08196),

547 [EEU99943.1](#) (ROSINTL182_08196), [EEU99894.1](#) (ROSINTL182_08199) and [EEU99897.1](#)
548 (ROSINTL182_08202). The authors declare that the data supporting the findings of this study are
549 available within the paper and the supplementary information or from the corresponding author on
550 request.

551

552 References

- 553 1. Nicholson, J. K. *et al.* Host-gut microbiota metabolic interactions. *Science* (80-.). **108**, 1262–1268 (2012).
- 554 2. Sonnenburg, J. L. & Bäckhed, F. Diet–microbiota interactions as moderators of human metabolism. *Nature* **535**,
555 56–64 (2016).
- 556 3. Marchesi, J. R. *et al.* The gut microbiota and host health: a new clinical frontier. *Gut* 1–10 (2015).
- 557 4. David, L. A. *et al.* Diet rapidly and reproducibly alters the human gut microbiome. *Nature* **505**, 559–563 (2013).
- 558 5. Desai, M. S. *et al.* A dietary fiber-deprived gut microbiota degrades the colonic mucus barrier and enhances
559 pathogen susceptibility. *Cell* **167**, 1339–1353.e21 (2016).
- 560 6. Cockburn, D. W. & Koropatkin, N. M. Polysaccharide degradation by the intestinal microbiota and its influence on
561 human health and disease. *J. Mol. Biol.* **428**, 3230–3252 (2016).
- 562 7. Xu, S. *et al.* Butyrate induces apoptosis by activating PDC and inhibiting complex I through SIRT3 inactivation.
563 *Signal Transduct. Target. Ther.* **2**, e16035 (2017).
- 564 8. Donohoe, D. R. *et al.* The warburg effect dictates the mechanism of butyrate-mediated histone acetylation and
565 cell proliferation. *Mol. Cell* **48**, 612–626 (2012).
- 566 9. Furusawa, Y. *et al.* Commensal microbe-derived butyrate induces the differentiation of colonic regulatory T cells.
567 *Nature* **506**, 254–254 (2014).
- 568 10. Morrison, D. J. & Preston, T. Formation of short chain fatty acids by the gut microbiota and their impact on human
569 metabolism. *Gut Microbes* **7**, 189–200 (2016).
- 570 11. Takahashi, K. *et al.* Reduced abundance of butyrate-producing bacteria species in the fecal microbial community in
571 Crohn’s disease. *Digestion* **93**, 59–65 (2016).

- 572 12. Qin, J. *et al.* A metagenome-wide association study of gut microbiota in type 2 diabetes. *Nature* **490**, 55–60 (2012).
- 573 13. Vrieze, A. *et al.* Transfer of intestinal microbiota from lean donors increases insulin sensitivity in individuals with
574 metabolic syndrome. *Gastroenterology* **143**, 913–916.e7 (2012).
- 575 14. Duncan, S. H., Hold, G. L., Barcenilla, A., Stewart, C. S. & Flint, H. J. *Roseburia intestinalis* sp. nov., a novel
576 saccharolytic, butyrate-producing bacterium from human faeces. *Int. J. Syst. Evol. Microbiol.* **52**, 1615–1620
577 (2002).
- 578 15. Louis, P. & Flint, H. J. Diversity, metabolism and microbial ecology of butyrate-producing bacteria from the human
579 large intestine. *FEMS Microbiol. Lett.* **294**, 1–8 (2009).
- 580 16. Van den Abbeele, P. *et al.* Butyrate-producing Clostridium cluster XIVa species specifically colonize mucins in an *in*
581 *vitro* gut model. *ISME J.* **7**, 949–61 (2013).
- 582 17. El Kaoutari, A., Armougom, F., Gordon, J. I., Raoult, D. & Henrissat, B. The abundance and variety of carbohydrate-
583 active enzymes in the human gut microbiota. *Nat. Rev. Microbiol.* **11**, 497–504 (2013).
- 584 18. Mirande, C. *et al.* Dietary fibre degradation and fermentation by two xylanolytic bacteria *Bacteroides xylanisolvens*
585 XB1AT and *Roseburia intestinalis* XB6B4 from the human intestine. *J. Appl. Microbiol.* **109**, 451–460 (2010).
- 586 19. Chassard, C., Goumy, V., Leclerc, M., Del’homme, C. & Bernalier-Donadille, A. Characterization of the xylan-
587 degrading microbial community from human faeces. *FEMS Microbiol. Ecol.* **61**, 121–131 (2007).
- 588 20. Sheridan, P. O. *et al.* Polysaccharide utilisation loci and nutritional specialisation in a dominant group of butyrate-
589 producing human colonic Firmicutes. *Microb. Genomics* **2**, (2016).
- 590 21. Selvendran, R. R. Chemistry of plant cell walls and dietary fibre. *Scand. J. Gastroenterol.* **5521**, 33–41 (1987).
- 591 22. Rogowski, A. *et al.* Glycan complexity dictates microbial resource allocation in the large intestine. *Nat. Commun.* **6**,
592 7481 (2015).
- 593 23. Zhang, M. *et al.* Xylan utilization in human gut commensal bacteria is orchestrated by unique modular
594 organization of polysaccharide-degrading enzymes. *Proc. Natl. Acad. Sci. U. S. A.* **111**, E3708–E3717 | (2014).
- 595 24. Lombard, V., Golaconda Ramulu, H., Drula, E., Coutinho, P. M. & Henrissat, B. The carbohydrate-active enzymes
596 database (CAZy) in 2013. *Nucleic Acids Res* **42**, (2014).
- 597 25. Kelly, G. *et al.* Structure of the cell-adhesion fragment of intimin from enteropathogenic *Escherichia coli*. *Nat*
598 *Struct Mol Biol* **6**, 313–318 (1999).

- 599 26. Ebbes, M. *et al.* Fold and Function of the InIB B-repeat. *J. Biol. Chem.* **286**, 15496–15506 (2011).
- 600 27. Karlsson, E. N. *et al.* The modular xylanase Xyn10A from *Rhodothermus marinus* is cell-attached, and its C-terminal
601 domain has several putative homologues among cell-attached proteins within the phylum Bacteroidetes. *FEMS*
602 *Microbiol. Lett.* **241**, 233–242 (2004).
- 603 28. Ejby, M. *et al.* An atp binding cassette transporter mediates the uptake of α -(1,6)-linked dietary oligosaccharides in
604 bifidobacterium and correlates with competitive growth on these substrates. *J. Biol. Chem.* **291**, 20220–20231
605 (2016).
- 606 29. Ejby, M. *et al.* Structural basis for arabinoxylo-oligosaccharide capture by the probiotic *Bifidobacterium animalis*
607 subsp. lactis BI-04. *Mol. Microbiol.* **90**, 1100–1112 (2013).
- 608 30. Honda, Y. & Kitaoka, M. A family 8 glycoside hydrolase from *Bacillus halodurans* C-125 (BH2105) is a reducing end
609 xylose-releasing exo-oligoxyylanase. *J. Biol. Chem.* **279**, 55097–55103 (2004).
- 610 31. Anand, S., Kaur, H. & Mande, S. S. Comparative *in silico* analysis of butyrate production pathways in gut
611 commensals and pathogens. *Front. Microbiol.* **7**, 1–12 (2016).
- 612 32. Duncan, S. H. *et al.* Wheat bran promotes enrichment within the human colonic microbiota of butyrate-producing
613 bacteria that release ferulic acid. *Environ. Microbiol.* **18**, 2214–2225 (2016).
- 614 33. Morrill, J. *et al.* The GH5 1,4- β -mannanase from *Bifidobacterium animalis* subsp. lactis BI-04 possesses a low-
615 affinity mannan-binding module and highlights the diversity of mannanolytic enzymes. *BMC Biochem.* **16**, 26
616 (2015).
- 617 34. Cockburn, D. W. *et al.* Molecular details of a starch utilization pathway in the human gut symbiont *Eubacterium*
618 *rectale*. *Mol. Microbiol.* **95**, 209–230 (2015).
- 619 35. Ze, X. *et al.* Unique organization of extracellular amylases into amyloosomes in the resistant starch-utilizing human
620 colonic firmicutes bacterium *Ruminococcus bromii*. *MBio* **6**, 1–11 (2015).
- 621 36. De Paepe, K., Kerckhof, F.-M., Verspreet, J., Courtin, C. M. & Van de Wiele, T. Inter-individual differences
622 determine the outcome of wheat bran colonization by the human gut microbiome. *Environ. Microbiol.* **0**, 1–17
623 (2017).
- 624 37. Mahowald, M. A. *et al.* Characterizing a model human gut microbiota composed of members of its two dominant
625 bacterial phyla. *Proc Natl Acad Sci U S A* **106**, 5859–5864 (2009).

- 626 38. Biely, P. *et al.* Mode of action of acetylxylan esterases on acetyl glucuronoxylan and acetylated oligosaccharides
627 generated by a GH10 endoxylanase. *Biochim. Biophys. Acta - Gen. Subj.* **1830**, 5075–5086 (2013).
- 628 39. Sørbotten, A., Horn, S. J., Eijsink, V. G. H. & Vårum, K. M. Degradation of chitosans with chitinase B from *Serratia*
629 *marcescens*. *FEBS J.* **272**, 538–549 (2005).
- 630 40. Cock, P. J. A. *et al.* Biopython: Freely available Python tools for computational molecular biology and
631 bioinformatics. *Bioinformatics* **25**, 1422–1423 (2009).
- 632 41. Kim, D. *et al.* TopHat2: accurate alignment of transcriptomes in the presence of insertions, deletions and gene
633 fusions. *Genome Biol.* **14**, R36 (2013).
- 634 42. Langmead, B. & Salzberg, S. L. Fast gapped-read alignment with Bowtie 2. *Nat Methods* **9**, (2012).
- 635 43. Anders, S., Pyl, P. T. & Huber, W. HTSeq-A Python framework to work with high-throughput sequencing data.
636 *Bioinformatics* **31**, 166–169 (2015).
- 637 44. Love, M. I., Huber, W. & Anders, S. Moderated estimation of fold change and dispersion for RNA-seq data with
638 DESeq2. *Genome Biol.* **15**, 550 (2014).
- 639 45. Dümmler, A., Lawrence, A.-M. & de Marco, A. Simplified screening for the detection of soluble fusion constructs
640 expressed in *E. coli* using a modular set of vectors. *Microb. Cell Fact.* **4**, 34 (2005).
- 641 46. Miller, G. L. Use of dinitrosalicylic acid reagent for determination of reducing sugar. *Anal. Chem.* **31**, 426–428
642 (1959).
- 643 47. Roe, J. H. & Rice, E. W. A photometric method for the determination of free pentoses in animal tissue. *J. Biol.*
644 *Chem.* **173**, 507–512 (1948).
- 645 48. Deschatelets, L. & Yu, E. K. C. A simple pentose assay for biomass conversion studies. *Appl. Microbiol. Biotechnol.*
646 **24**, 379–385 (1986).
- 647 49. Dilokpimol, A. *et al.* Enzymatic synthesis of β -xylosyl-oligosaccharides by transxylosylation using two β -xylosidases
648 of glycoside hydrolase family 3 from *Aspergillus nidulans* FGSC A4. *Carbohydr. Res.* **346**, 421–429 (2011).
- 649 50. Govind, V., Young, K. & Maudsley, A. A. Corrigendum: Proton NMR chemical shifts and coupling constants for brain
650 metabolites. Govindaraju V, Young K, Maudsley AA, *NMR Biomed.* 2000; 13: 129-153. *NMR Biomed.* **28**, 923–924
651 (2015).
- 652 51. Zhang, H., Neal, S. & Wishart, D. S. RefDB: A database of uniformly referenced protein chemical shifts. *J. Biomol.*

653 *NMR* **25**, 173–195 (2003).

654 52. Takeo, K. Affinity electrophoresis: Principles and applications. *Electrophoresis* **5**, 187–195 (1984).

655 53. Scott, K. P., Martin, J. C., Duncan, S. H. & Flint, H. J. Prebiotic stimulation of human colonic butyrate-producing
656 bacteria and bifidobacteria, in vitro. *FEMS Microbiol. Ecol.* **87**, 30–40 (2014).

657

658 Acknowledgements

659 We wish to thank Bernard Henrissat, architecture et fonction des macromolécules biologiques,
660 CNRS, Aix-Marseille University and the curator of CAZy, for his advice and discussions on the
661 assignment of the novel CBMx and the esterase. We thank Dr. Madhav, Yadav, United States
662 Department of Agriculture, Agricultural Research Service for the kind gift of cornbran xylan, and
663 BioCHOS AS (Ås, Norway) for providing the chitooligo (CHOS) sample. Marzanna Due, Thanh Holm
664 Madsen and Camilla Aaarup Christensen are thanked for technical help in cloning recombinant
665 proteins and the performance of binding experiments. We also wish to thank Alexander Schultz,
666 Helle Juel Martens and Micheal Hansen, PLEN, University of Copenhagen for the use of confocal
667 laser scanning microscopy in the initial microscopy experiments. This project was funded by a
668 Graduate School DTU Scholarship, Lyngby, Denmark. Additional fundings were from the Danish
669 Research Council for Independent Research, Natural Sciences (DFF, FNU) by a Research Project 2
670 grant (Grant ID: 4002-00297B), a BIONÆR project (grant numbers 244259) and the Norwegian NMR
671 Platform, NNP (FLA) from the Research Council of Norway and (226244).

672

673 Author contributions

674 Growth analysis was performed by M.L.L. Transcriptomic analysis was by M.L.L, C.W, and D.A.E.
675 Enzyme characterization was by M.L.L., M.E., S.S.P, F.L.A and B.W. qPCR was by M.L.L and M.I.B.
676 Microscopy was by M.L.L and C.S. Experiments were designed by M.L.L and M.A.H. The manuscript

677 written by M.L.L and M.A.H. with contributions from T.R.L, B.W. and F.L.A. Figures were prepared by
678 M.L.L.

679

680 Competing interests

681 The authors declare no competing financial interests.

682

683 Corresponding authors

684 Correspondence to Maher Abou Hachem (maha@bio.dtu.dk)

685

686 Figure legends

687 **Figure 1 Growth of *R. intestinalis* and induction of extracellular activity.** (a) Schematic representation of cereal
688 arabinoxylan and glucuronoxylan present in dicots cell wall, e.g. in fruits and vegetables. (b) Growth level for 18 hours on
689 xylans, oligosaccharides thereof and monosaccharide components, with glucose as a control. Green: $OD_{600\text{ nm}}$ increase >1.0
690 for soluble substrates and pH drop > 0.3 for insoluble xylans; yellow: $0.3 < \Delta OD_{600\text{ nm}} < 0.5$; red: $\Delta OD_{600\text{ nm}} < 0.1$. Asterisks
691 indicate insoluble xylans (c) Growth curves on glucose, wheat arabinoxylan (WAX), birch glucuronoxylan (BGX) and a no
692 carbon source control. (d) Growth on insoluble wheat arabinoxylan (InWAX) and oat spelt xylan (OSX). All growth
693 measurements are means of triplicates with standard deviations. (e) Xylanase activity of *R. intestinalis* cells grown on
694 glucose, xylo-oligosaccharides, BGX and WAX for 18 hours. (f) Cells grown on BGX were washed (PBS buffer ± 1.5 M NaCl)
695 and xylanase activity was measured in wash and cell fractions to verify localization of the enzymes. Xylanase activity was
696 measured using the DNS reducing sugar assay and data are triplicates with standard deviations.

697 **Figure 2 The core xylan utilization apparatus of *R. intestinalis*.** (a) The RNA-Seq heatmap depicts Log₂ fold changes of the
698 top upregulated xylan utilization genes expressed by cells grown on xylose (X1), wheat arabinoxylan (WAX) and birch
699 glucuronoxylan (BGX) relative to glucose (Glc). Formal locus tag numbers ROSINTL182_xxxxx are abbreviated with the last
700 numbers after the hyphen. Signal peptides (SP) were predicted using SignalP v.3.0. (b) Gene expression depicted as mean
701 of the normalized Deseq2 gene counts for the core xylan utilization genes shown in (a). (c) Extracellular localization of

702 *RiXBP* and *RiXyn10A*, the solute binding protein of the xylo-oligosaccharide specific ABC transporter and the xylanase,
703 respectively, were visualized by fluorescence microscopy of *R. intestinalis* cells using primary antibodies targeting these
704 two proteins. No auto fluorescence was observed for cells without primary antibody (data not shown).

705 **Figure 3 A novel low affinity xylan binding module mediates extended xylan binding to the xylanase *RiXyn10A*. (a)**

706 Domain organization of *RiXyn10A* and truncated variants. Carbohydrate binding module (CBM), novel CBM (CBMx),
707 bacterial Ig-like domain group 2 (BIG2), Listeria-Bacteroides repeat domain (LBR). (b,c) Xylanase activity of *RiXyn10A* on
708 WAX and BGX assayed by HPAEC-PAD and thin layer chromatography, respectively. Peaks in 3b eluting after X6 are likely to
709 be decorated xylo-oligosaccharides. (d) Hydrolysis kinetic parameters of *RiXyn10A*, *RiXyn10A*ΔCBMx and *RiXyn10A*-cata
710 towards WAX and BGX. Kinetics of the *RiXyn10A*-cata are not modelled by the Michaelis-Menten expression and catalytic
711 efficiencies are estimated from linear regression of initial rate data. Data are means of triplicates with standard deviations.
712 (e) Binding parameters of *RiXyn10A* and variants towards oligosaccharides. Dissociation constants (K_D) determined by
713 surface plasmon resonance (SPR) are means of a duplicate with the standard deviations. * K_D (mg mL⁻¹) from affinity
714 electrophoresis (AE), and ** K_D from isothermal titration calorimetry (ITC). (f) Binding of *RiXyn10A*-CBMx to the negative
715 control (no polysaccharide), WAX or BGX xylans analyzed using AE. Lanes 1+2; *RiXyn10A*-CBMx (3.0 μg), Lane 3; β-
716 lactoglobulin negative control (1.5 μg), M; marker. (g) Binding isotherms of *RiXyn10A*-CBMx to xylo-oligosaccharides. Solid
717 lines are fits of a one binding site model to the SPR sensograms.

718 **Figure 4 Intracellular xylo-oligosaccharide depolymerization. (a)** α-glucuronidase and α-L-arabinofuranosidase activity on

719 WAX and BGX for *RiAgu115A* and *RiAbf43A*, respectively, based on HPAEC-PAD analysis. (b) Time-resolved NMR for *RiAXE*
720 enzymatic deacetylation of acetylated birch glucuronoxylan (AcBGX) treated with *RiXyn10A* and *RiAgu115A*. Deacetylation
721 time course for the first 30 min and after 18 h (green 0 min, purple 30 min, orange 18 h). All verified signals with 2-*O*-
722 acetylation decreased faster in the initial phase of the reaction. The proton spectra of the acetylated region show nearly
723 complete deacetylation of the sample after 18 h. The signal at 2.13 ppm is likely attributed to another acetylated sugar
724 residue. Acetyl groups are designated as: C2, 2-*O*-acetylated xylose; C3, 3-*O*-acetylated xylose, C23, 2,3-di-*O*-acetylated
725 xylose; C3-MeGlcA; 4-*O*-methylglucuronic acid 2-*O*-substituted and 3-*O*-acetylated xylose; C23(2); signal for the 2-*O*-
726 acetylated of C23. The assignment of the acetylated sugar signals were based on homo and heteronuclear NMR correlation
727 experiments (Supplementary Fig. 7) (c-f) Hydrolysis products from AcBGX by (c) *RiXyn10A*, (d) *RiXyn10A* and *RiAgu115A*, (e)
728 *RiXyn10A* and *RiAXE*, (f) *RiXyn10A*, *RiAgu115A* and *RiAXE*. Enzyme action was analyzed by MALDI-ToF MS; Xylo-
729 oligosaccharides decorated with acetyl and methylglucuronic acid are in green, acetyl in blue, methylglucuronic acid in red,
730 no sidechains in orange. Di-sodium adducts of a methylglucuronic acid decorated oligosaccharides (diamonds) are colored
731 as their corresponding single sodium adducts.

732 **Figure 5 Model for xylan utilization by *R. intestinalis* and competition assay with *Bacteriodes ovatus*. (a)** *RiXyn10A* on the
733 cell surface efficiently captures diet-derived acetylated arabinoxylan and acetylated glucuronoxylan by its CBMs and
734 hydrolyzes it into linear and decorated xylo-oligosaccharides, which are subsequently captured by *RiXBP* for uptake into
735 the cytoplasm. Internalized xylo-oligosaccharides are debranched and hydrolyzed into monosaccharides and acetate.
736 Xylose and arabinose are converted to xylulose 5-phosphate before entering the pentose phosphate pathway, whereas
737 methyl-glucuronic acid is converted to 2-oxo-3-deoxygalactonate 6-phosphate. These precursors enter glycolysis, which
738 generates pyruvate, some of which is used to synthesize butyrate³¹ that is externalized. The asterisk next to *RiAbf43A*
739 indicates that the enzyme is able to hydrolyze both α -1,2 and α -1,3 linked L-arabinose. Black solid arrows show steps
740 established or confirmed in this study. Grey solid arrows indicate steps described in literature. Grey dashed arrows indicate
741 that H₂ and butyrate are externalized by unknown mechanisms. To make the model more general for the *R. intestinalis*
742 species, the second less upregulated extracellular xylanase *RiXynB*, unique for the L1-82 strain, is not included in the
743 model, although it is expressed at the cell surface. **(b-d)** Growth of monoculture and co-cultures of *R. intestinalis* and *B.*
744 *ovatus* on WAX, InWAX and BGX. Data are means of a triplicate with standard deviations. **(e-h)** Time course relative
745 abundance during growth of co-cultures on xylans and xylotetraose (X4) determined by qPCR. All data are means of a
746 biological triplicate.

747

748 Tables

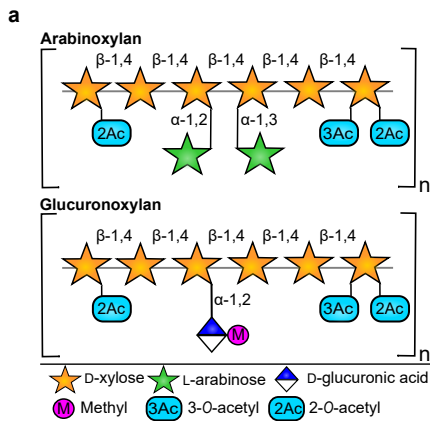
749

Table 1: Binding energetics of the transport protein *RiXBP* to xylo-oligosaccharides determined by ITC

Ligand	K_D (μ M)	N_0	ΔH (kcal/mol)	$T\Delta S$ (kcal/mol)	ΔG (kcal/mol)	
X6	112.7 \pm 7.5	1.19 \pm 0.14	-9.01 \pm 1.3	-3.6	-5.4	★★★★★★★★
X5	10.3 \pm 1.5	0.86 \pm 0.01	-13.54 \pm 0.3	-6.7	-6.8	★★★★★★
X4	16.5 \pm 2.6	0.68 \pm 0.02	-12.8 \pm 0.4	-6.3	-6.5	★★★★★
X3	225.7 \pm 14.5	0.58 \pm 0.23	-21.1 \pm 9.5	-16.1	-5.0	★★★★
X2	n.d.					★★
AX3	215.5 \pm 95.2	0.26 \pm 0.04	-44.3 \pm 7.1	-39.4	-4.9	★★★ ★
AX4	6.8 \pm 1.2	0.58 \pm 0.01	-12.3 \pm 0.2	-7.0	-5.3	★★★★★ ★

Data are means of a duplicate experiment with standard deviations. n.d. indicates that no binding was observed. AX3 is an arabino-xylotriase with a non-reducing end arabinosyl and AX4 is an arabino-xylotetraose with an arabinosyl decoration at the penultimate position from the non-reducing end (see Supplementary Fig. 5h,i).

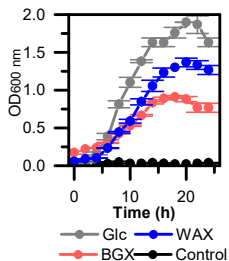
756



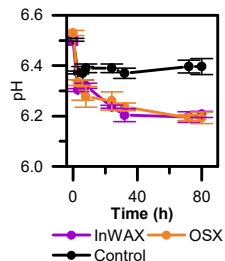
b

Substrate	Growth
Glucose (Glc)	
Arabinose (A1)	
Glucuronic acid (GlcA)	
Xylose (X1)	
Xylobiose (X2)	
Xylotriose (X3)	
Xylotetraose (X4)	
Xylohexaose (X6)	
Corn cob xylooligosaccharides (CCXOS)	
Wheat arabinoxylan (WAX)	
Birchwood glucuronoxylan (BGX)	
Acetylated birchwood glucuronoxylan (AcBGX)	
Corn bran arabinoglucuronoxylan (CBX)	
Insoluble wheat arabinoxylan (InWAX)*	
Oat spelt xylan (OSX)*	

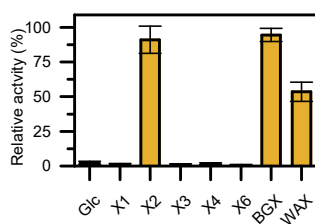
c Growth on soluble xylans



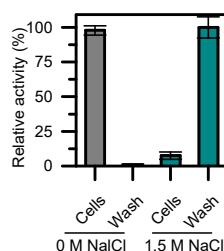
d Growth on insoluble xylans



e Induction of xylanase activity

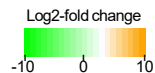
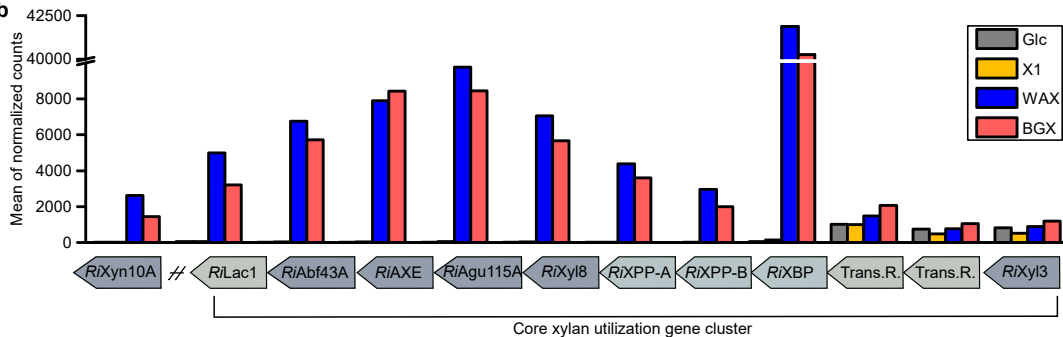
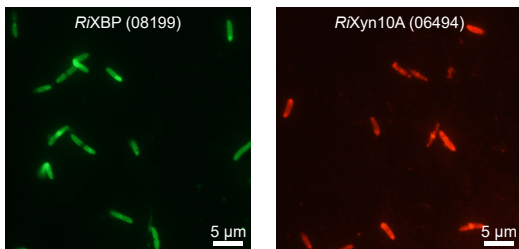


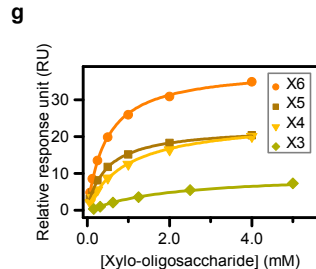
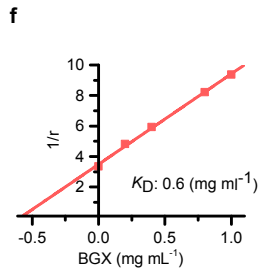
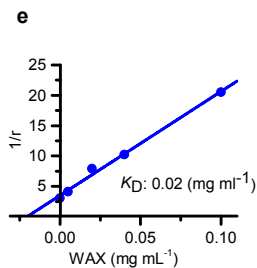
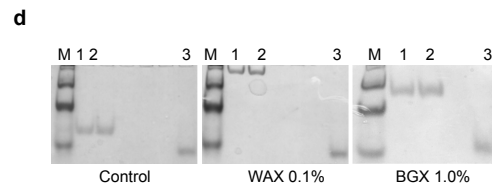
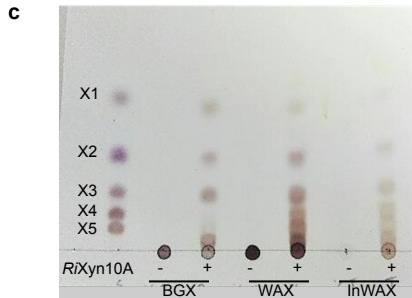
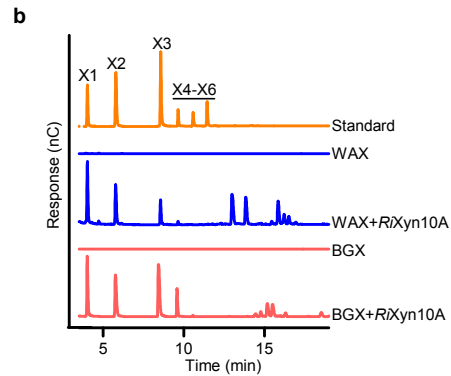
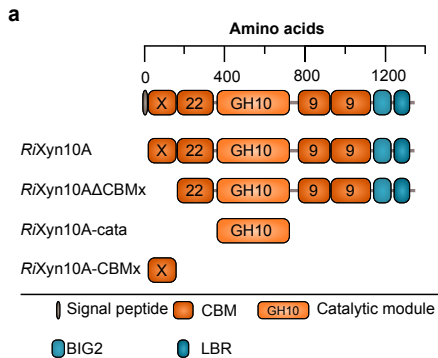
f Cell attachment of xylanase activity

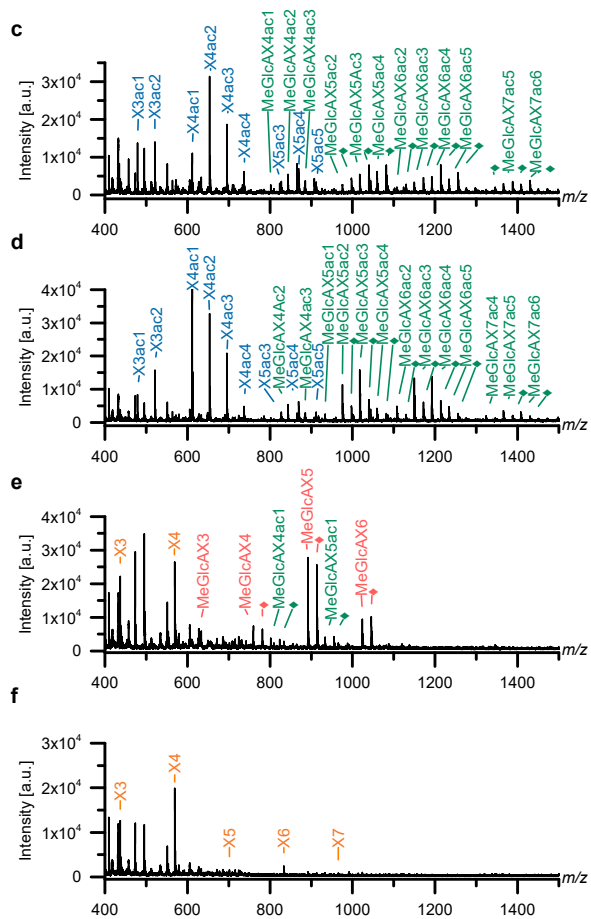
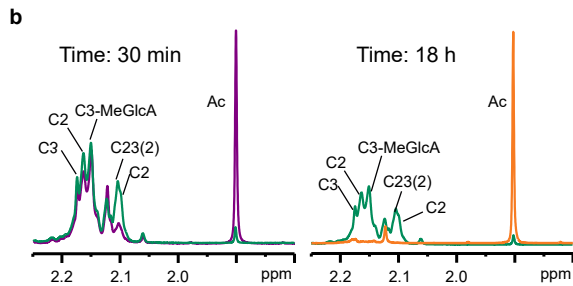
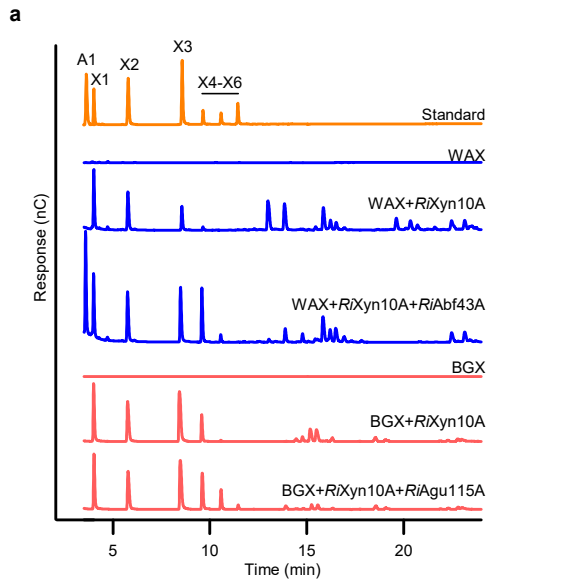


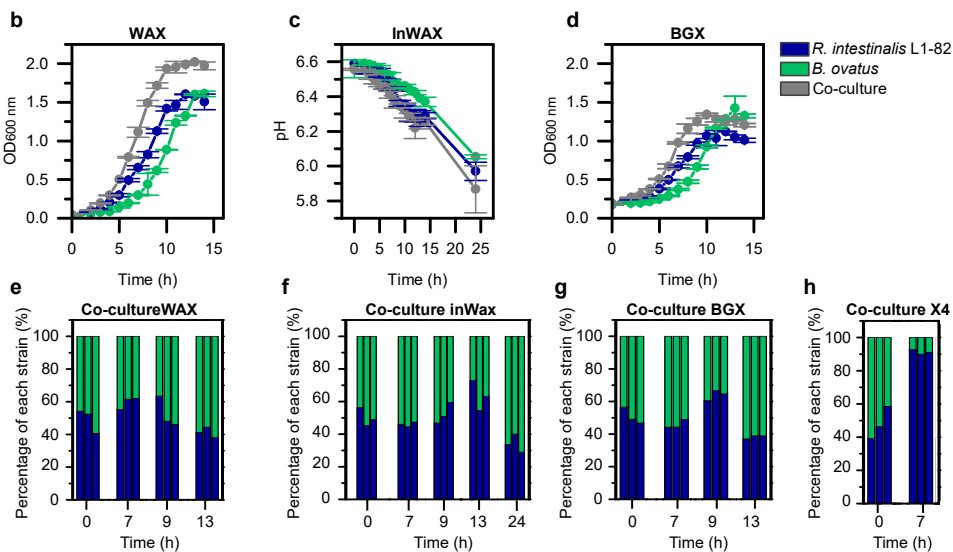
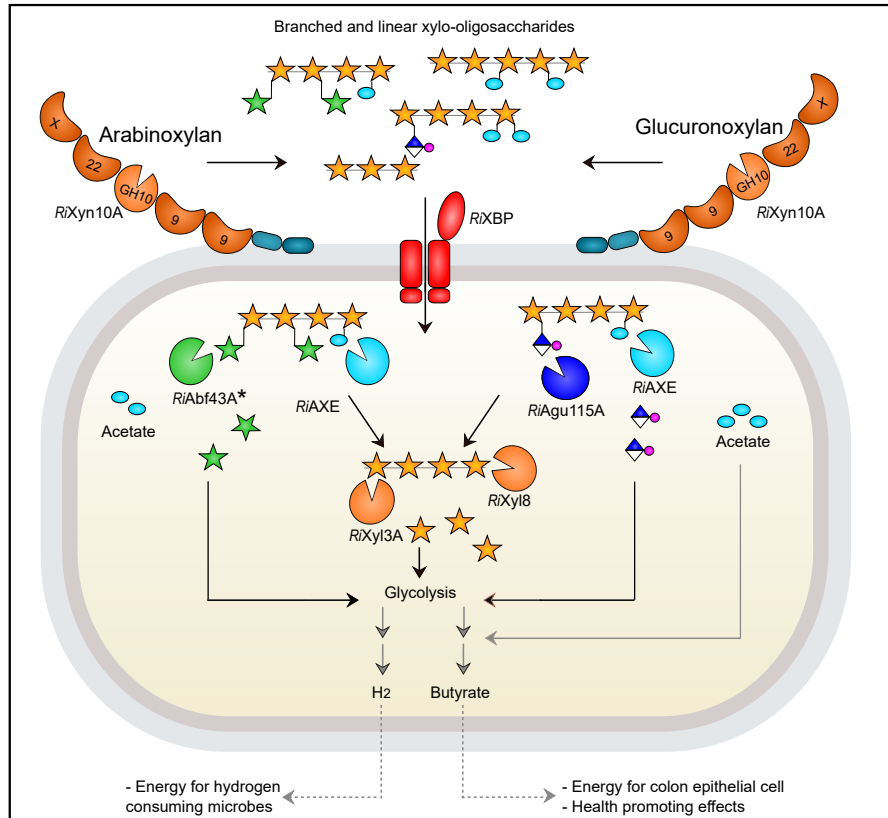
a

Locus ID	Log2-fold change			SP	Protein	Annotation
	X1/Glc	WAX/Glc	BGX/Glc			
06494	-1.04	7.00	6.17	Yes	<i>RiXyn10A</i>	Endo-1,4- β -xylanase
08192	-0.46	6.46	5.82	No	<i>RiLac1</i>	Transcriptional regulator, LacI family
08193	0.04	8.69	8.45	No	<i>RiAbf43A</i>	α -L-arabinofuranosidase
08194	0.24	8.78	8.88	No	<i>RiAXE</i>	Acetyl xylan esterase
08195	0.63	8.55	8.35	No	<i>RiAgu115A</i>	Xylan α -1,2-glucuronidase
08196	0.78	8.60	8.29	No	<i>RiXyl8</i>	Reducing-end-xylose releasing exo-oligoxylanase
08197	0.91	8.71	8.43	No	<i>RiXPP-A</i>	ABC transporter, permease protein
08198	0.03	8.89	8.33	No	<i>RiXPP-B</i>	ABC transporter, permease protein
08199	0.49	9.12	9.07	Yes	<i>RiXBP</i>	ABC transporter, xylan binding protein
08200	0.28	0.46	0.96	No		Transcriptional regulator
08201	-0.25	-0.07	0.40	No		Transcriptional regulator
08202	-0.22	0.02	0.44	No	<i>RiXyl3A</i>	Xylan 1,4- β -xylosidase

**b****c**







Supplementary Table 2. Modular organization of GH10 xylanases from human gut Firmicutes and Bacteroidetes.

Phylum	Family	Strain	Accession number	Length (AA)	CBMs	
Firmicutes	Lachnospiraceae	<i>Roseburia intestinalis</i> L1-82	ROSINTL182_06494	1356	X, 22, 9, 9	
			ROSINTL182_6338-9	601		
		<i>Roseburia intestinalis</i> XB6B4	CBL13458.1	1356	X, 22, 9, 9	
		<i>Roseburia intestinalis</i> M50/1	n.a.	1356	X, 22, 9, 9	
		<i>Roseburia faecis</i> M72	CRL32809.1	1380	X, 22, 9, 9	
		<i>Eubacterium rectale</i> T1-815	CRL34489.1	1028	X, 9, 9	
		<i>Butyrivibrio fibrisolvens</i> 16/4	CBK74925.1	1153	9	
			CBK75021.1	690	13, 2	
		<i>Hungatella hathewayi</i>	CUO52114.1	421		
		<i>Ruminococcus gnavus</i>	WP_064787180.1	394		
	Ruminococcaceae	<i>Ruminococcus champanellensis</i> 18P13	CBL16579.1	633	22	
			CBL17682.1	1268	22, 22, 6	
		<i>Ruminococcus callidus</i> ATCC 27760	ERJ94429.1	1158	22, 22, 9	
			ERJ87773.1	630	22	
			ERJ97032.1	382	22	
		Bacteroidetes	Bacteroidaceae	<i>Bacteroides ovatus</i>	EDO13863.1	372
EDO10007.1 ¹	376					
EDO14247.1	573					
EDO10010.1 ¹	740				4, 4	
EDO14052.1	584					
EDO10798.1	750					
<i>Bacteroides intestinalis</i> DSM 17393	EDV05054.1				782	4, 4
	EDV05072.1 ²				746	4, 4
	EDV03684.1				738	
<i>Bacteroides xyloxylicus</i> 16/4	EDV05059.1				910	
	EDV07678.1			725		
	EDV07007.1 ²			899		
	<i>Bacteroides xylanisolvens</i> XB1A			CBK67953.1 ³	754	4, 4
CBH32823.1				378		

AA: amino acids, n.a.: GH10 is present, but not assigned in the genome,

1. Rogowski, A. *et al.* Glycan complexity dictates microbial resource allocation in the large intestine. *Nat. Commun.* **6**, 7481 (2015).
2. Zhang, M. *et al.* Xylan utilization in human gut commensal bacteria is orchestrated by unique modular organization of polysaccharide-degrading enzymes. *Proc. Natl. Acad. Sci. U. S. A.* **111**, E3708-E3717 (2014)
3. Despres, J. *et al.* Xylan degradation by the human gut *Bacteroides xylanisolvens* XB1AT involves two distinct gene clusters that are linked at the transcriptional level. *BMC Genomics* **17**, 326 (2016).

Supplementary Table 3. Thermodynamic parameters and dissociation constant for RfXyn10A-CBMx determined by ITC.

Ligand	K_D (μ M)	N_0	ΔH (kcal/mol)	$T\Delta S$ (kcal/mol)	ΔG (kcal/mol)
X6	413 \pm 125	0.74 \pm 0.04	-19.9 \pm 1.2	-15.3	-4.6

Data are from one experiment and binding parameters are reported with the error of the fit to the binding isotherm.

Supplementary Table 4. Homologs of CBMx identified in genomes of taxonomically related taxa to *R. intestinalis*.

Strain	Accession number	Query cover	E-value	Identity
<i>Roseburia intestinalis</i> XB6B4	CBL13458.1	100%	4e-85	100%
<i>Eubacterium rectale</i> _T1815	CRL34489.1	89%	5e-36	55%
<i>Butyrivibrio</i> sp. LC3010	WP_026509692.1	92%	1e-07	36%
<i>Roseburia faecis</i> M72	CRL32809.1	93%	9e-12	36%
<i>Bacterium enrichment culture clone</i> MC3F	AFU34339.1	86%	3e-07	30%
<i>Lachnospiridium phytofermentans</i> ISDg	ABX41884.1	84%	5e-07	26%
<i>Clostridium</i> sp. KNHs205	WP_033165005.1	88%	1e-06	28%
<i>Butyrivibrio</i> sp. INlla14	SCX91715.1	63%	2e-06	32%
<i>Lachnospiraceae bacterium</i> YSD2013	SCX14282.1	73%	1e-05	34%
<i>Butyrivibrio</i> sp. ob235	SEK63083.1	76%	2e-04	30%
<i>Butyrivibrio</i> sp. VCD2006	WP_026526370.1	72%	3e-04	27%

Supplementary Table 5. Kinetic parameters of RiAgu115A.

Substrate	K_M (mg mL ⁻¹)	k_{cat} (s ⁻¹)	k_{cat}/K_M (mL mg ⁻¹ s ⁻¹)
BeGX	n.d.	n.d.	2
BeGX + RiXyn10A	12 ± 3	395 ± 34	33

n.d.: Low affinity and lack of curvature of the Michaelis Menten plots precluded reliable determination of kinetic parameters. Catalytic efficiencies are from the slope of the initial rates versus substrate concentration. Data are means of a triplicate with standard deviations.

Supplementary Table 6. Kinetics of RiAbf43A.

Substrate	K_M (mM)	k_{cat} (s ⁻¹)	k_{cat}/K_M (s ⁻¹ mM ⁻¹)
AX4	0.8 ± 0.1	20 ± 1	25
	K_M (mg mL ⁻¹)	k_{cat} (s ⁻¹)	k_{cat}/K_M (mL mg s ⁻¹)
WAX	6.3 ± 0.4	12 ± 0	1.9

Data are means of a triplicate with standard deviations.

Supplementary Table 7. Kinetics *RiXyl3A*.

Substrate	K_M (mM)	k_{cat} (s ⁻¹)	k_{cat}/K_M (s ⁻¹ mM ⁻¹)
X2	2.7 ± 0.4	57 ± 3	21
X3	3.4 ± 0.3	60 ± 2	18
X4	2.4 ± 0.4	32 ± 2	13
X5	2.6 ± 0.5	36 ± 1	14
X6	2.1 ± 0.2	30 ± 1	15

Data are means of a triplicate with standard deviations.

Supplementary Table 8. Kinetics *RiXyl8*.

Substrate	K_M (mg/mL)	k_{cat} (S ⁻¹)	k_{cat}/K_M (s ⁻¹ ·mM ⁻¹)
X3	4.8 ± 1.0	1208 ± 124	251.7
X4	5.1 ± 1.5	892 ± 131	174.9

Data are means of a triplicate with standard deviations.

Supplementary Table 9. Deacetylation activity of *RiAXE* on acetylated xylans and aryl acetate.

Substrate	Enzyme(s)	V (μM s ⁻¹)	V/[E] (s ⁻¹)
AcBGX	<i>RiAXE</i>	2.5	39.1
	<i>RiAXE</i> + <i>RiXyn10A</i>	3.2	50
	<i>RiAXE</i> + <i>RiXyn10A</i> + <i>RiAgu115A</i>	2.8	43.8
AcSpruce mannan	<i>RiAXE</i>	0.2	3.1
pNP-acetate	<i>RiAXE</i>	4.7 ^a ± 0.1	n.d.
Autolysis		0.07	n.d.

V: rate, V/[E]: normalized rate by enzyme concentration estimated from NMR experiments. ^aThe activity on paranitrophenyl acetate (pNP-acetate) is expressed in U mg⁻¹.

Supplementary Table 10. Assignment of chemical shifts for xylan deacetylation by *RiAXE*.

Structural unit	Assignment						
	H-1; C-1	H-2; C-2	H-3; C-3	H-4; C-4	H-5; C-5	H-6; C-6	Ac-H; C
X	4.42; 105.4	3.19; 75.4	3.53; 76.4	3.78; 79.2	n.d	n.d	-
C2	4.68; 102.6	4.69; 76.1	3.79; 74.2	3.86; 78.9	n.d	n.d	2.10; 23.1 /2.16; 23.1
C3	4.47; 104.3	3.37; 75.4	4.89; 79.9	3.78; 79.1	n.d	n.d	2.17; 23.2
C23	4.81; 102.2	4.81; 74.2	5.17; 74.1	4.05; 77.9	n.d	n.d	(2) 2.10; 22.9/ (2) 2.12; 23.0
C3MeGlcA	4.57; 104.2	3.48; 73.6	4.98; 78.1	3.94; 78.1	n.d	n.d	2.15; 23.3
MeGlcA	5.17; 96.6	3.56; 74.4	3.53; 73.3	n.d	n.d	n.d	-
α	5.18; 94.8	3.56; 74.2	3.53; 73.7	n.d	n.d	n.d	-
β	4.56; 99.3	3.25; 76.7	3.52; 77.9	3.72; 79.7	n.d	n.d	-

Supplementary Table 11. Esterase activity for RiAXE measured using MALDI-TOF.

	AcBGX	AcAspen xylan	AcSpruce mannan	Cellulose mono acetate	AcChitin	InWAX
<i>RiAXE</i>	++	++	+	+	-	-
<i>RiAXE + RiAgu115A</i>	+++	n.d.	n.d.	n.d.	n.d.	n.d.

+++ : complete deacetylation, ++:almost complete acetylation (1 ≥ acetyl/oligosaccharide),

+: minor deacetylation (1-2 acetyl/oligosaccharide), -: no deacetylation). Experiments performed twice.

Supplementary Table 12. Xylan hydrolysis kinetics of RiXyn10B.

Substrate	K_M (mg mL ⁻¹)	k_{cat} (s ⁻¹)	k_{cat}/K_M (mL mg ⁻¹ s ⁻¹)
BGX	n.d.	n.d.	9.8
WAX	4.4 ± 0.8	413 ± 32	94
InWAX	n.d.	n.d.	2.3

n.d.: Low affinity and lack of curvature of the Michaelis Menten plots precluded reliable determination of the kinetic parameters and the catalytic efficiencies are determined from the slope of the initial rate data versus substrate concentration. Data are reported as means of triplicates with standard deviations

Supplementary Table 13. Cloning and mutagenesis primers^{a,b}.

Gene	Accession number	Name	Orientation	Sequence (5' -> 3')
ROSINTL182_06494 (AA27-1356)	EEV01588.1	RiXyn10A	Forward	TTTCAGGGCGCCATGGGGTAAAAAAGTTTTACTGCAGAT
ROSINTL182_06494 (AA27-1356)	EEV01588.1	RiXyn10A	Reverse	GACGGAGCTCGAATTTTACTACTACTGATCTTTATCTCTTTGCA
ROSINTL182_06494 (AA156-1356)	EEV01588.1	RiXyn10AΔCBMx	Forward	TTTCAGGGCGCCATGGCAGGAGCAGCGCATGCA
ROSINTL182_06494 (AA156-1356)	EEV01588.1	RiXyn10AΔCBMx	Reverse	GACGGAGCTCGAATTTTACTACTACTGATCTTTATCTCTTTGCA
ROSINTL182_06494 (AA349-754)	EEV01588.1	RiXyn10A-cata	Forward	TTTCAGGGCGCCATGCTATTGAGAAGGACATCCCGGA
ROSINTL182_06494 (AA349-754)	EEV01588.1	RiXyn10A-cata	Reverse	GACGGAGCTCGAATTTTGGATGCATCTACATACGCCCA
ROSINTL182_06494 (AA27-165)	EEV01588.1	RiXyn10A-CBMx	Forward	TTTCAGGGCGCCATGGGGTAAAAAAGTTTTACTGCAGAT
ROSINTL182_06494 (AA27-165)	EEV01588.1	RiXyn10A-CBMx	Reverse	GACGGAGCTCGAATTTTATCCCCAATTTTGCA
ROSINTL182_08193	EEU99940.1	RiAbf43A	Forward	AGGAGATATACCATGAGTATAGCAAAGATCCGGTTC
ROSINTL182_08193	EEU99940.1	RiAbf43A	Reverse	GGTGGTGGTCTCGAAACCCGGTATTCCCTCATA
ROSINTL182_08194	EEU99941.1	RiAXE	Forward	AGGAGATATACCATGAGTGGACCTGTGGCA
ROSINTL182_08194	EEU99941.1	RiAXE	Reverse	GGTGGTGGTCTCGAATTCACATAGCCAAAACCAA
ROSINTL182_08195	EEU99942.1	RiAgu115A	Forward	TTTCAGGGCGCCATGGAAGCAATTTGGTAAAGGATC
ROSINTL182_08195	EEU99942.1	RiAgu115A	Reverse	GACGGAGCTCGAATTTTATCATCTGTTCTGCTCCTCT
ROSINTL182_08196	EEU99943.1	RiXyl8	Forward	AGGAGATATACCATGAAAAGAGGAGCGTTTGAGA
ROSINTL182_08196	EEU99943.1	RiXyl8	Reverse	GGTGGTGGTCTCGAATAAATCTATAATTGCCGCTCAG
ROSINTL182_08199	EEU99894.1	RiXBP	Forward	TTTCAGGGCGCCATGGAAACAAAGCAGCCG
ROSINTL182_08199	EEU99894.1	RiXBP	Reverse	GACGGAGCTCGAATTTTATTACTGATATTTTTGCTTCTC
ROSINTL182_08202	EEU99897.1	RiXyl3A	Forward	AGGAGATATACCATGGAATTAATCAGAATACAGAAAACTG
ROSINTL182_08202	EEU99897.1	RiXyl3A	Reverse	GGTGGTGGTCTCGAATAACATCAGACTTCCACTGTTT
ROSINTL182_06338/ ROSINTL182_06339	EEV01752.1/ EEV01731.1	RiXyn10B	Forward	TTTCAGGGCGCCATGGCTGGCGAGGAAAATG
ROSINTL182_06338/ ROSINTL182_06339	EEV01752.1/ EEV01731.1	RiXyn10B	Reverse	GACGGAGCTCGAATTTTACTATTTATCAGAATGAAATAAATTTCAA

^aBold nucleotides indicate the sequences annealing to the vector.

^bUnderlined nucleotides indicate the changed codon and italics indicate the changed bases.

Supplementary Table 14. qPCR primers use.

Target bacteria	Orientation	Sequence (5' -> 3')	Reference
<i>Roseburia</i> spp.	Forward	TACTGCATTGGAAACTGTCC	1
<i>Roseburia</i> spp.	Reverse	CGGCACCGAAGAGCAAT	1
<i>Bacteroides</i> spp.	Forward	CGATGGATAGGGTTCTGAGAGGA	2
<i>Bacteroides</i> spp.	Reverse	GCTGGCACGGAGTTAGCCGA	2
Universal primer	Forward	ACTCCTACGGGAGGCAGCAGT	3
Universal primer	Reverse	GTATTACCGCGCTGCTGGCAC	3

1. Larsen, N. *et al.* Gut microbiota in human adults with type 2 diabetes differs from non-diabetic adults. *PLoS One* **5**, e9085 (2010).

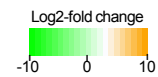
2. Bergström, A. *et al.* Introducing GUT Low-Density Array (GULDA)-a validated approach for qPCR-based intestinal microbial community analysis. *FEMS Microbiol. Lett.* **337**, 38–47 (2012).

3. Walter, J. *et al.* Detection and identification of gastrointestinal *Lactobacillus* species by using denaturing gradient gel electrophoresis and species-specific PCR primers. *Appl. Environ. Microbiol.* **66**, 297–303 (2000).

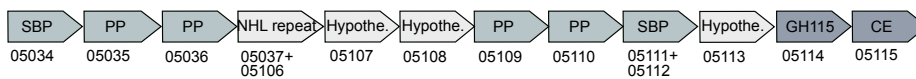
Supplementary Figures

a

Locus ID	Log2-fold change			SP	Protein	Annotation
	X1/Glc	WAX/Glc	BGX/Glc			
05034	-0.84	6.48	5.54	Yes	SBP	ABC transporter, solute-binding protein
05035	-0.79	5.99	5.44	No	PP	ABC transporter, permease protein
05036	-0.80	6.04	5.26	No	PP	ABC transporter, permease protein
05037+05106	-0.33	6.44	5.95	Yes		NHL repeat protein
05107	-1.48	5.98	5.53	No		Hypothetical protein
05108	-0.42	5.91	5.48	No		Hypothetical protein
05109	-0.61	5.87	4.92	No	PP	ABC transporter, permease protein
05110	-0.63	5.11	3.92	No	PP	ABC transporter, permease protein
05111+05112	0.34	5.73	5.07	Yes	SBP	ABC transporter, solute-binding protein
05113	-0.77	4.95	4.78	No		Hypothetical protein
05114	-0.95	4.09	4.08	No	GH115	Xylan α -1,2-glucuronidase
05115	-0.73	4.35	4.17	No	CE	Putitativ esterase

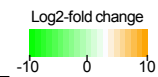


b

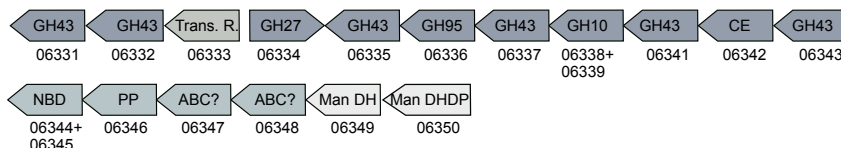


c

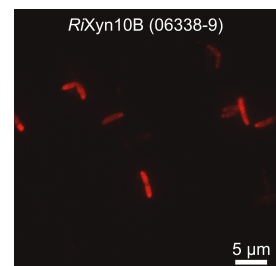
Locus ID	Log2-fold change			SP	Protein	Annotation
	X1/Glc	WAX/Glc	BGX/Glc			
06331	-0.63	5.26	4.76	No	GH43	β -xylosidase/ α -L-arabinofuranosidase
06332	-1.60	5.46	4.74	No	GH43	β -xylosidase/ α -L-arabinofuranosidase
06333	-0.70	0.44	2.24	No	AraC	Transcriptional regulator
06334	-1.22	1.03	2.44	No	GH27	α -galactosidase/ β -L-arabinopyranosidase
06335	-0.69	3.58	3.44	No	GH43	β -xylosidase/ α -L-arabinofuranosidase
06336	-1.04	3.61	3.21	No	GH95	α -L-galactosidase/ α -L-fucosidase
06337	-0.57	3.45	4.08	No	GH43	β -xylosidase/ α -L-arabinofuranosidase
06338+06339	-0.99	3.47	3.62	Yes	RiXyn10B	Endo-1,4- β -xylanase
06341	-1.12	4.09	3.80	No	GH43	β -xylosidase/ α -L-arabinofuranosidase
06342	-1.32	4.28	4.07	No	CE1	Esterase
06343	-1.23	4.49	4.21	Yes	GH43	β -xylosidase/ α -L-arabinofuranosidase
06344+06345	-1.57	4.49	4.68	No	ABC-NBD	ABC transporter, nucleotide binding domain
06346	-2.45	5.12	4.74	No	ABC-PP	ABC transporter, permease protein
06347	-2.38	5.49	5.35	No		Hypothetical ABC transporter
06348	-1.62	4.52	4.04	No		Hypothetical ABC transporter
06349	-0.95	6.49	5.44	No	UxuA	Mannonate dehydratase
06350	-1.50	5.84	5.12	No	UxuB	Mannitol/D-arabinitol dehydrogenase domain protein



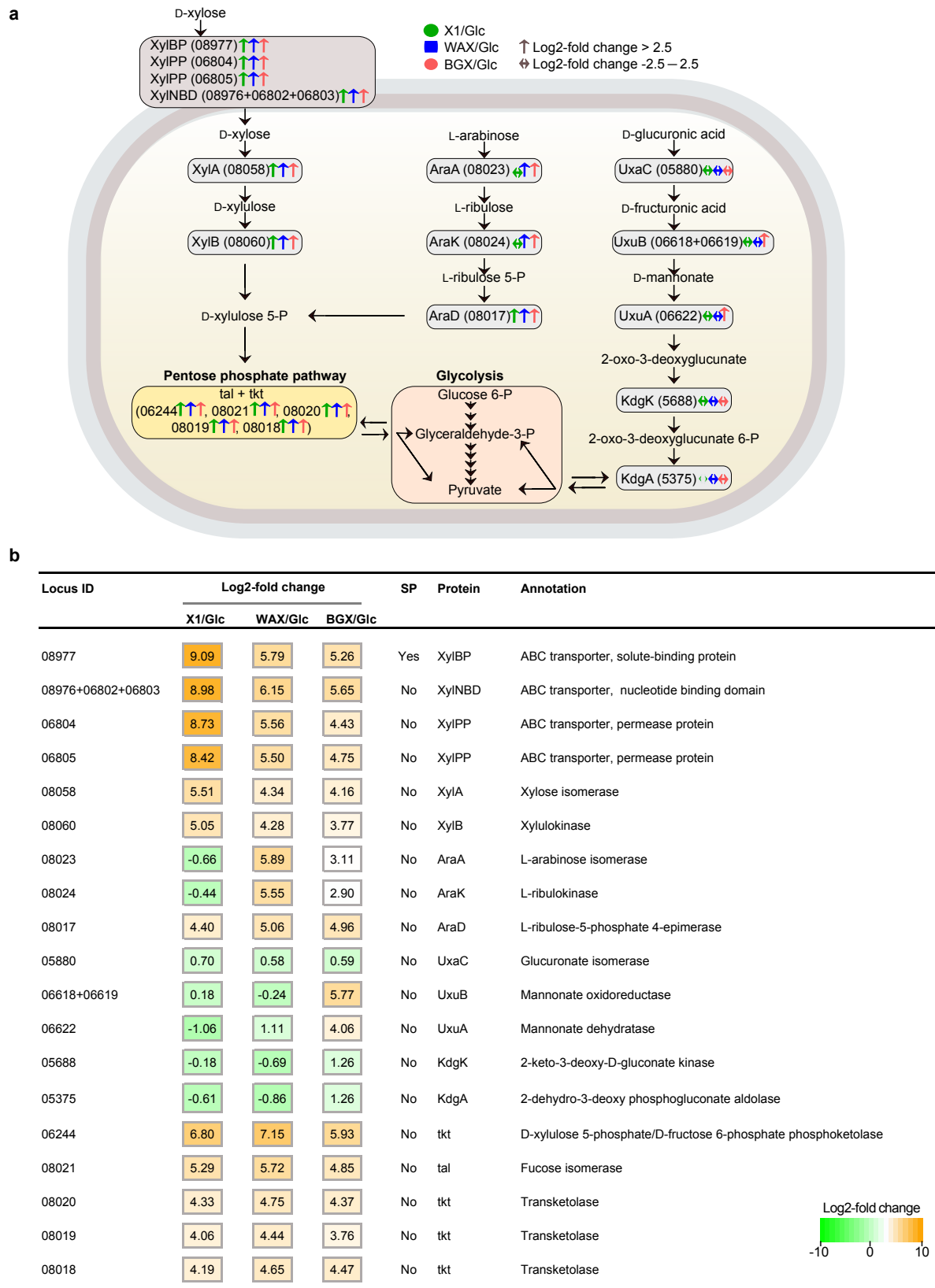
d



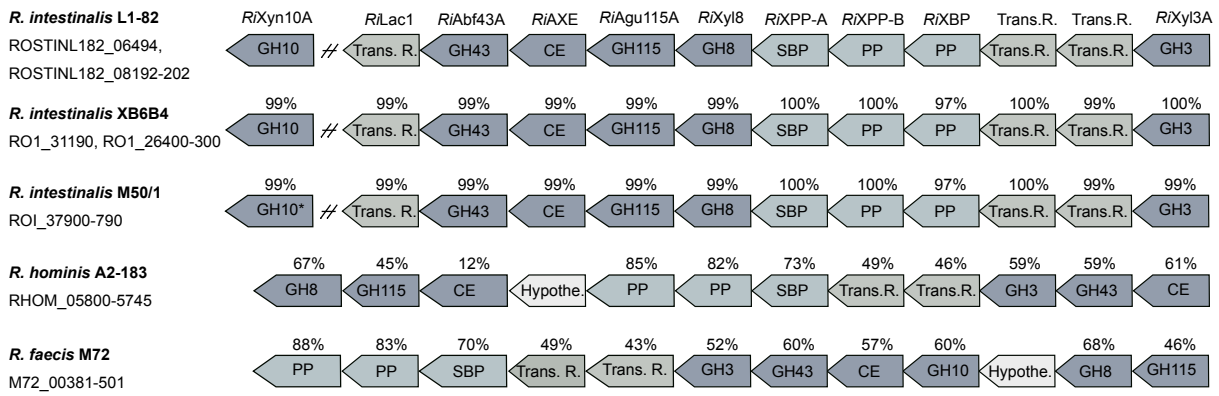
e



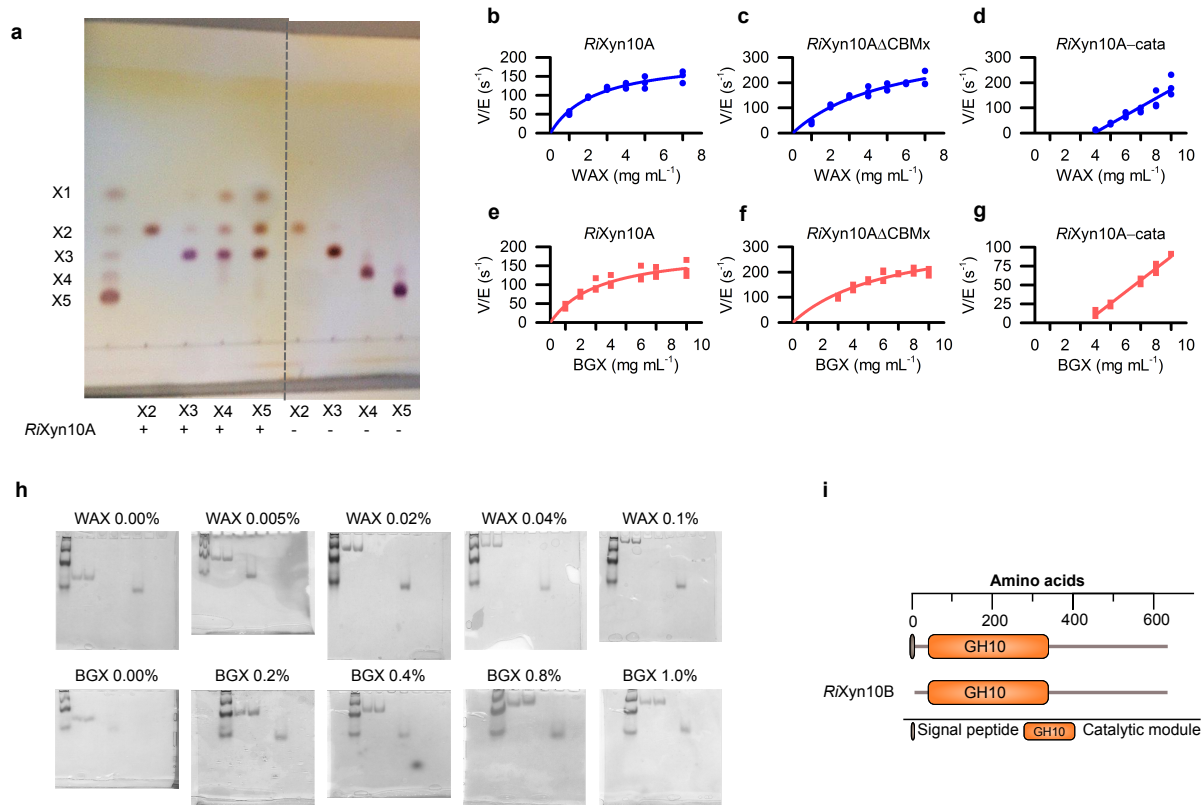
Supplementary Figure 1 *R. intestinalis* L1-82 unique xylan upregulated loci. **(a)** Upregulation of a putative xylan metabolism gene cluster unique for the *R. intestinalis* L1-82 strain on xylan. **(b)** Organization of genes in (a). **(c)** Second unique *R. intestinalis* L1-82 gene cluster upregulated on xylan. **(d)** Organization of putative xylan-metabolism genes upregulated in (c). **(e)** Fluorescence microscopy of *R. intestinalis* grown on xylan showing the extracellular localization of RiXyn10B. Experiments were performed three times and locus IDs ROSINTL182_xxxxx are abbreviated with the last numbers after the hyphen. Signal peptides (SP) were predicted using SignalP v.3.0. Genes residing between two contigs have two locus IDs.



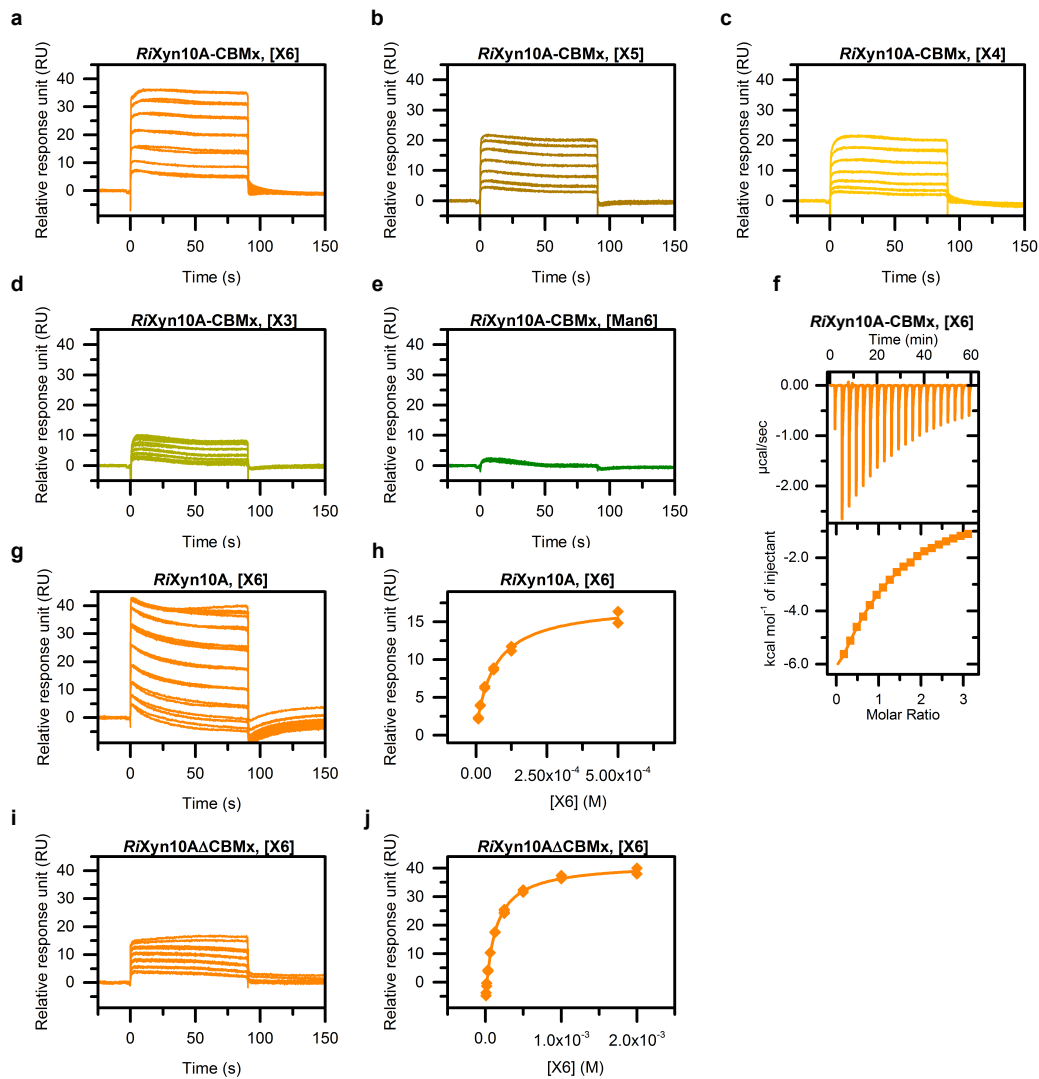
Supplementary Figure 2 *R. intestinalis* L1-82 xylose metabolism. (a) Proposed model for the metabolism of the monosaccharides xylose, arabinose and glucuronic acid in *R. intestinalis* L1-82 based on the RNA-seq data in Supplementary Table 1, and literature. (b) Upregulation of xylose import and metabolism genes in the model. The RNA-Seq heatmap depicts Log2-fold changes of genes expressed by cells grown on xylose (X1), wheat arabinoxylan (WAX) and birch glucuronoxylan (BGX) relative to glucose (Glc). Locus numbers ROSINTL182_xxxx are abbreviated with the last numbers after the hyphen.



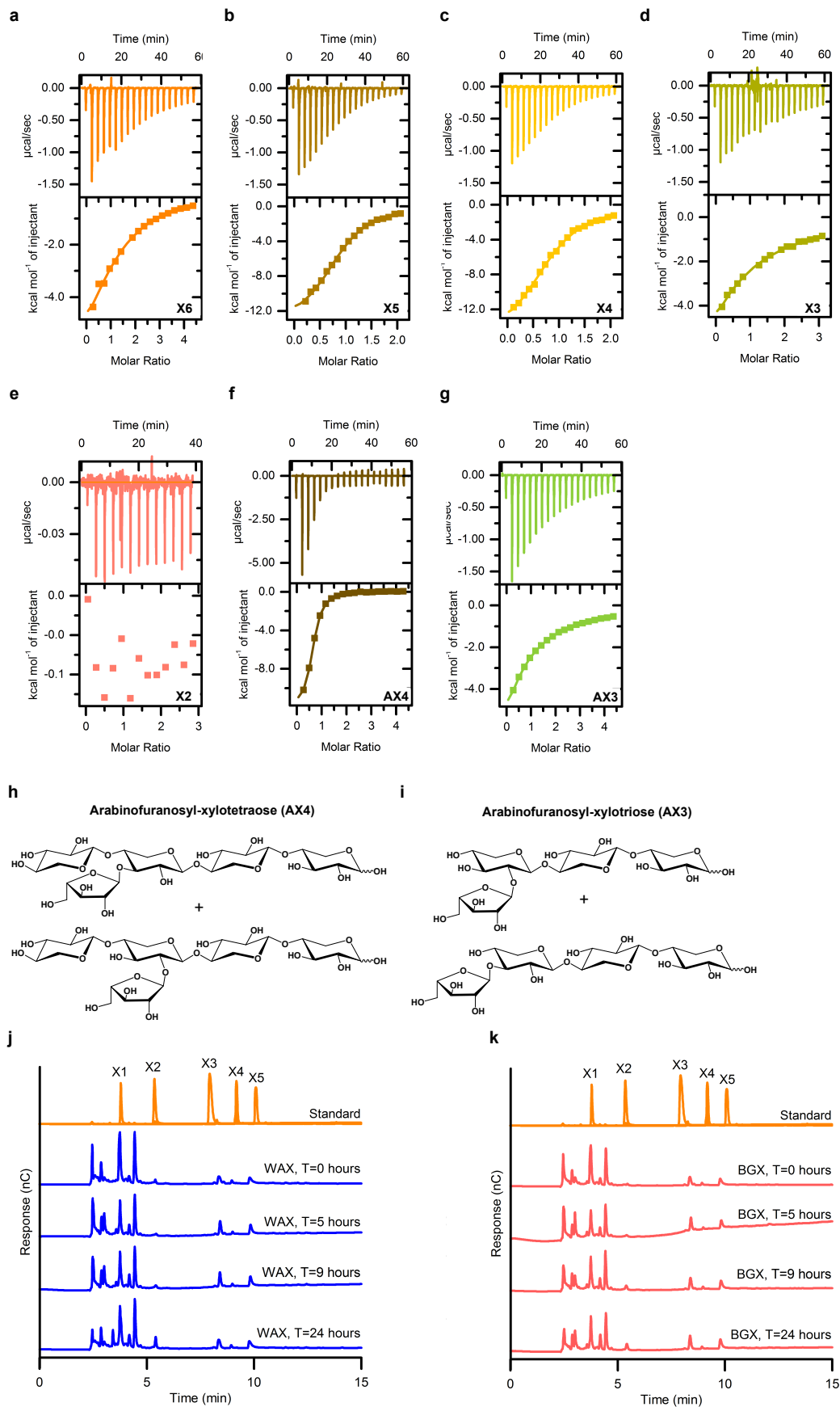
Supplementary Figure 3 Conservation of *R. intestinalis* core xylan utilization genes within the *Roseburia* genus. Genes are denoted according to their protein products; glycoside hydrolase (GH), carbohydrate esterase (CE), transcriptional regulators (Trans.R.), ABC transporter solute binding protein (SBP), ABC transporter permease protein (PP) and hypothetical proteins (Hypothe.). Sequence identities to *R. intestinalis* L1-82 genes are shown above the genes; Locus IDs for the genes are denoted under the respective strains. The asterisk indicates that the GH10 is not assigned in the genome.



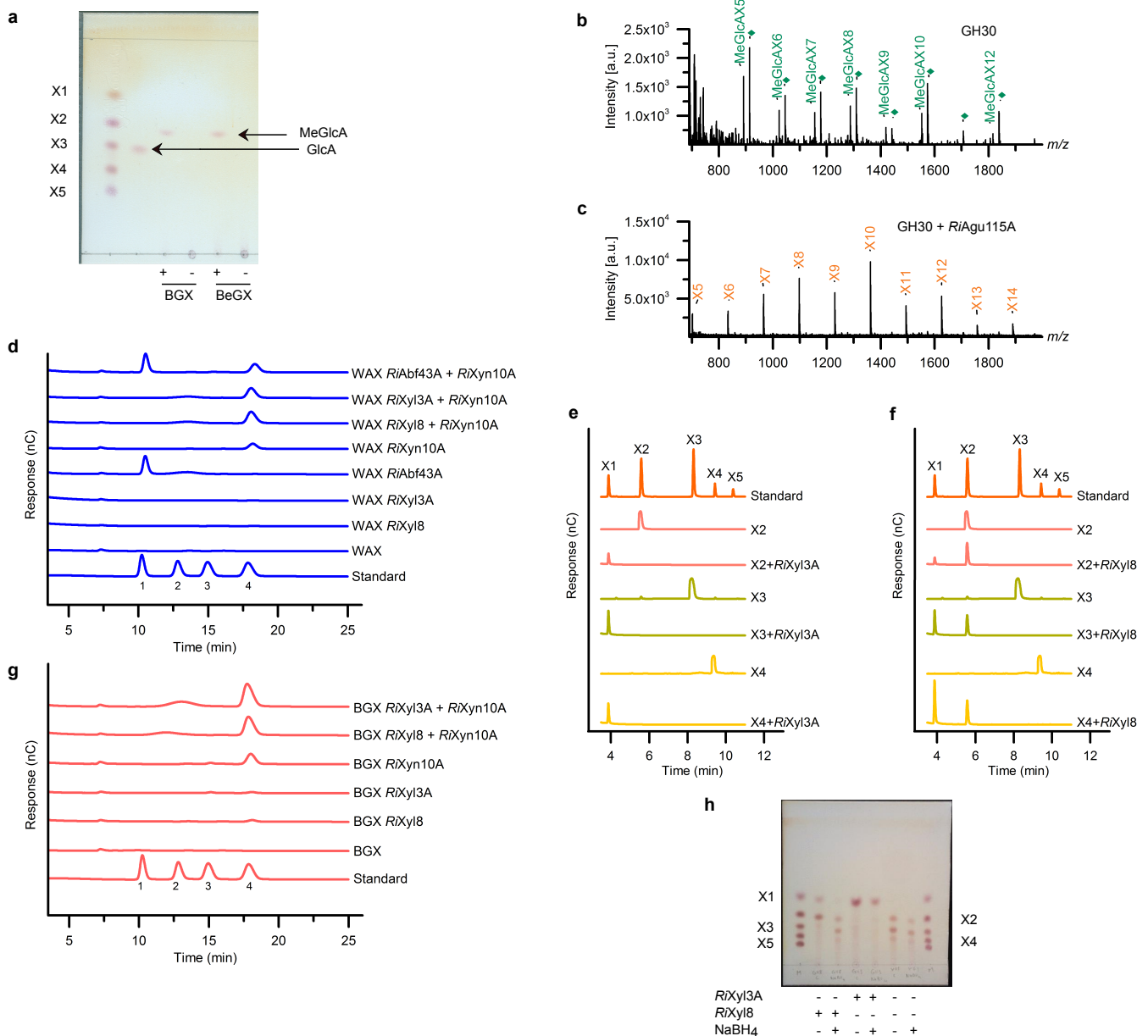
Supplementary Figure 4 Properties of the extracellular xylanases from *R. intestinalis* (a) Action patterns of *RiXyn10A* on X2–X5 analyzed by TLC; +: reaction with enzyme, -: controls without enzyme. The dotted line indicates that lanes not relevant to the figure were spliced out for clarity. (b–g) Hydrolysis kinetics of *RiXyn10A*, *RiXyn10AΔCBMx* lacking the N-terminal module and *RiXyn10A-cata*, the catalytic module on WAX, and BGX. (h) Binding of xylans to *RiXyn10A*-CBMx by affinity gel electrophoresis using native polyacrylamide gels with different concentrations of WAX (0.0–0.1% w/v) or BGX (0.0–1.0% w/v). No polysaccharides were added to the control. Lane 1+2; *RiXyn10A*-CBMx (3.0 μg), Lane 3 β-lactoglobulin (1.5 μg), M; marker. (i) Domain organization of the xylanase *RiXyn10B* encoded by a locus upregulated on xylan and which is unique for the *R. intestinalis* L1-82 strain used in the present study (Supplementary Fig. 1c–d). The bottom cartoon represents the recombinant enzyme. Experiments in (a) and (h) are performed twice and in triplicates for (b–g).



Supplementary Figure 5 Binding of CBMx and *RiXyn10A* to xylo-oligosaccharides. (a-e) Reference and blank corrected sensograms depict binding of xylo-oligosaccharides (X3-X6) and mannohexaose (Man6) as negative control to CBMx (*RiXyn10A*-CBMx) using SPR analysis. **(f)** ITC analysis of CBMx binding to X6. **(g,i)** Reference and blank corrected SPR sensograms depicting the binding of X6 to *RiXyn10A* and *RiXyn10A*ΔCBMx respectively. **(h,j)** One binding model fitted to the binding isotherms from the sensograms in (g,i). The experiments were in triplicates, except for the ITC run once.

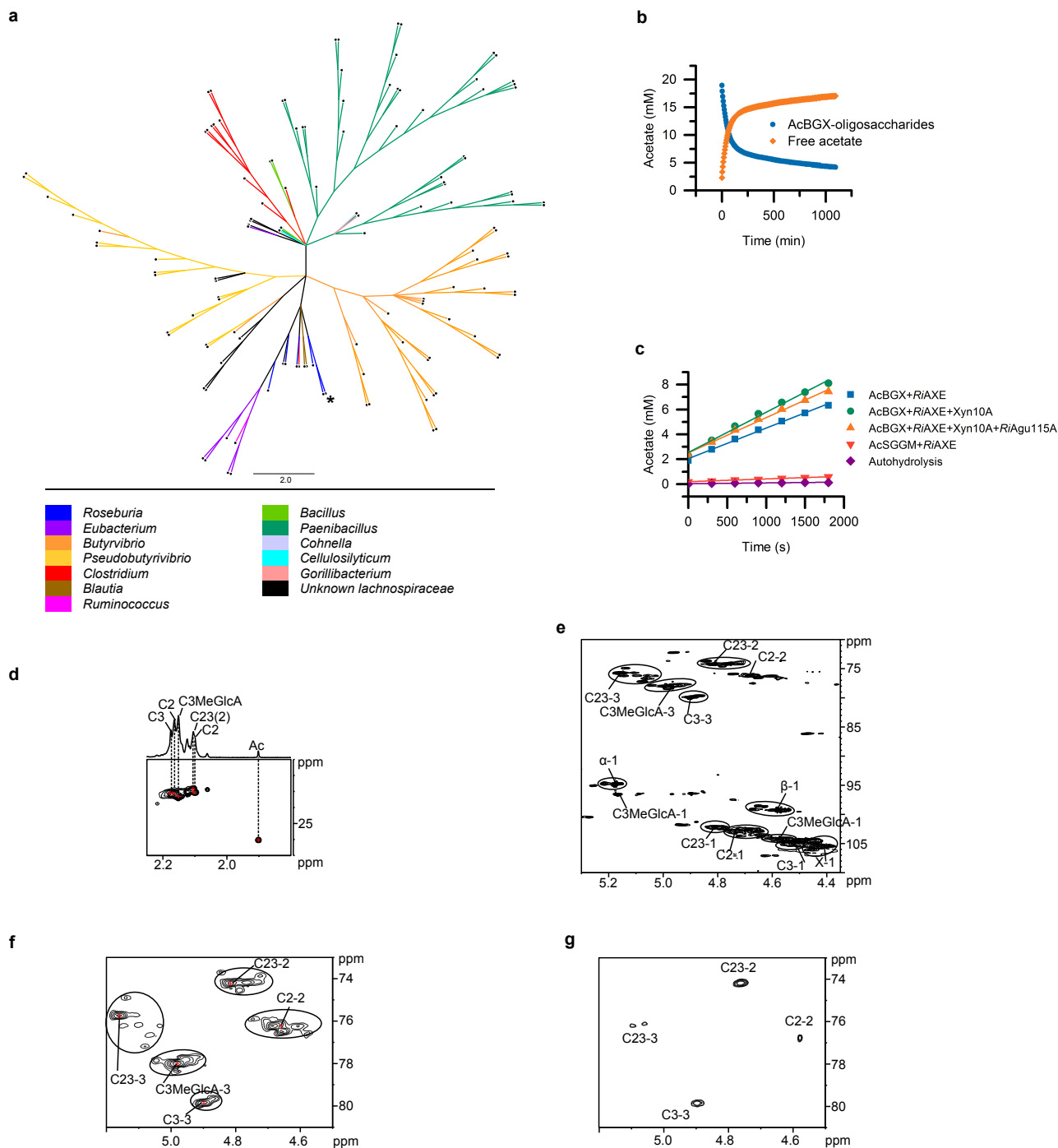


Supplementary Figure 6 Binding preference of *RixBP* associated to the xylo-oligomer ABC transporter of *R. intestinalis*. (a-g) ITC analysis of *RixBP* binding to linear and branched xylo-oligosaccharides. (h,i) Structures of the branched arabinosylated xylo-oligosaccharides AX4 and AX3, which are mixtures with arabinofuranosyl decoration either at the C2 or C3 of xylosyl units. (j,k) Time course HPAEC-PAD analysis of culture supernatants of *R. intestinalis* grown in YCFA with 0.5% WAX or BGX. The observed peaks between 0 and 5 minutes are likely unutilized medium components. Experiments in (a-g) are duplicates, and in (j,k) from a duplicate.



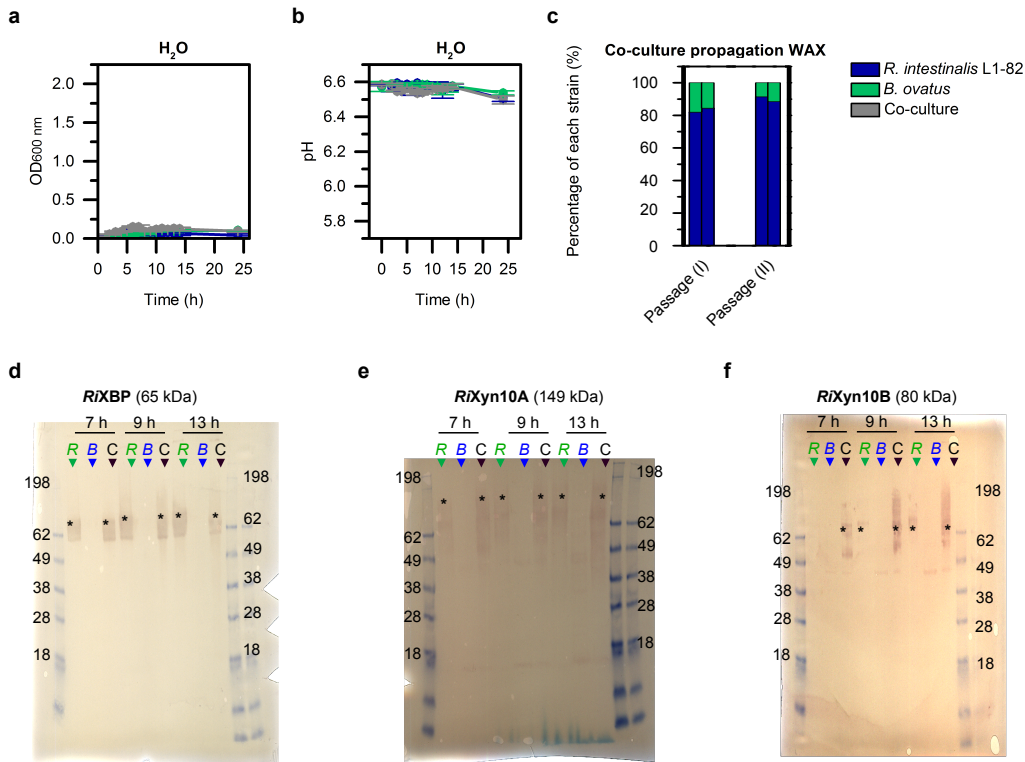
Supplementary Figure 7 Intracellular xylo-oligosaccharide degrading enzymes from *R. intestinalis* (a) TLC analysis of the release of 4-*O*-methylglucuronic acid (MeGlcA) from BGX and BeGX by *RiAgu115A*. Glucuronic acid (GlcA) is used as standard. (b,c) Activity of *RiAgu115A* on a GH30-hydrolyzed BeBGX monitored using MALDI-ToF MS; (b) is the GH30 control and (c) is the treatment with GH30 and *RiAgu115A*. Activity indicates *RiAgu115A* releases MeGlcA from the penultimate xyloxy to the reducing end in xylo-oligosaccharides based on the GH30 strict specificity¹, whereas a GH10 generates xylo-oligosaccharides with a MeGlcA substitution at the non-reducing end². This data shows that the *RiAgu115A* is able to act on both internal and terminal non-reducing end substitutions on glucuronoxylan-derived xylo-oligosaccharides. Di-sodium adducts of MeGlcA decorated oligomers (diamonds) are colored as their corresponding single sodium adducts. (d,g) Monosaccharide hydrolysis products from enzymatic treatment of WAX and BGX with *RiXyn10A*, *RiAbf43A*, *RiXyl3A* and *RiXyl8* by HPAEC-PAD. Standards were 1; arabinose, 2; galactose, 3; glucose, 4; xylose. (e,f) *RiXyl3A* and *RiXyl8* hydrolysis of xylo-oligosaccharides analyzed with HPAEC-PAD. (h) β -xylosidase activity for *RiXyl3A* and *RiXyl8* towards xylo-oligosaccharides (XOS) by TLC. The + and - indicate the presence and absence of the different components, respectively. Lack of activity on substrate reduced with NaBH₄ (converts reducing end unit to its alditol) provided evidence that *RiXyl8* acts on the reducing end as the alditol is not accommodated in the active site. Experiments are performed in duplicates.

1. St John, F. J., Hurlbert, J. C., Rice, J. D., Preston, J. F. & Pozharski, E. Ligand bound structures of a glycosyl hydrolase family 30 glucuronoxylan xylanohydrolase. *J. Mol. Biol.* **407**, 92–109 (2011).
2. Dodd, D. & Cann, I. K. Enzymatic deconstruction of xylan for biofuel production. *Glob Chang. Biol Bioenergy* **1**, 2–17 (2009).



Supplementary Figure 8 Activity, specificity and taxonomic distribution of the novel xylan acetyl esterase *RiAXE*. (a) Phylogenetic tree of *RiAXE* and homologs identified by a BLASTP search against the non-redundant database. Sequences with coverage >86% and identity >42% were selected. All sequences were from Firmicutes members. The resulting 131 protein sequences were aligned using Muscle¹ and a phylogenetic tree constructed by the maximum likelihood algorithm in MEGA7². Bootstraps were performed with 500 replicates. The phylogenetic tree was visualized using Figtree (<http://tree.bio.ed.ac.uk/software/figtree>). Asterisk indicates position of *RiAXE*. (b) Time course deacetylation of AcBGX treated with *RiXyn10A* and *RiAgu115A* by *RiAXE* determined by NMR. (c) Rates of deacetylation by *RiAXE* on AcBGX and AcSpruce mannan (AcSGGM) in D₂O, which may influence absolute reaction rates. (d) ¹³C HSQC spectrum of *RiXyn10A* treated AcBGX showing the acetyl region and with the 1D proton projection. (e) same as (d) but showing the spectral region for anomeric and *O*-acetylated xylose signals. *RiXyn10A* treatment enhances signal-to-noise of resonances in the NMR spectra for the assignment and increases the total number of observable individual signals. (f, g) ¹³C HSQC spectra for *O*-acetylated regions before (f) and after (g) deacetylation by *RiAXE*. Nearly complete deacetylation of AcBGX is reached during the time resolved NMR experiment. Chemical shifts of the most dominating signal for the monosaccharide residues mark by "+", peaks encircled by dotted lines indicate cluster of chemical shifts likely to belong to the same type of monosaccharide residue as dominating signal.

1. Edgar, R. C. MUSCLE: multiple sequence alignment with high accuracy and high throughput. *Nucleic Acids Res.* **32**, 1792–1797 (2004).
2. Kumar, S., Stecher, G. & Tamura, K. MEGA7: Molecular evolutionary genetics analysis version 7.0 for bigger datasets. *Mol. Biol. Evol.* **33**, msw054 (2016).



Supplementary Figure 9 Co-culture experiment with *R. intestinalis* and *B. ovatus*. (a-b) Growth curves for monoculture and co-cultures after growth of *R. intestinalis* and *B. ovatus* with water as controls instead of carbon source. (c) Relative abundance determined by qPCR in a propagation experiment with co-cultures on WAX. After 9 hours of growth, the co-culture was passaged into fresh media, passage (I) (start OD_{600} nm=0.01). This culture was grown for 12 hours and passaged into fresh media again (passage II). The western blots were carried out with (d) anti-*RiXBP*, (e) anti-*RiXyn10A*, (f) anti-*RiXyn10B*. R: *R. intestinalis*, B: *B. ovatus*, C: co-culture of *R. intestinalis* and *B. ovatus*. Asterisk denotes the position of the band based on theoretical molecular mass. The molecular markers size is shown in kDa. Lower molecular mass signals than expected indicate proteolytic cleavage occurring particularly with the multi-modular *RiXyn10A*. Experiments are performed in biological triplicates in (a-c) and in duplicates in (d-f).